

2006

LIBRARY
Michigan State
University

This is to certify that the dissertation entitled

#### **HYBRID CONTROL OF FLEXIBLE STRUCTURES**

presented by

SHAHIN SABOKDAST NUDEHI

has been accepted towards fulfillment of the requirements for the

Ph.D. degree. in MECHANICAL ENGINEERING

**M**ajor Professor's Signaturé

Date

MSU is an Affirmative Action/Equal Opportunity Institution

## PLACE IN RETURN BOX to remove this checkout from your record. TO AVOID FINES return on or before date due. MAY BE RECALLED with earlier due date if requested.

DATE DUE	DATE DUE	DATE DUE
\$2 0 4 0 3 NAY 0 2 2007		
N.S. V Z 2007		
	· ·	
		ONE autopolitana Dua ladd a 15

2/05 c:/CIRC/DateDue.indd-p.15

#### HYBRID CONTROL OF FLEXIBLE STRUCTURES

By

Shahin Sabokdast Nudehi

#### **A DISSERTATION**

Submitted to
Michigan State University
in partial fulfillment of the requirements
for the degree of

DOCTOR OF PHILOSOPHY

Department of Mechanical Engineering

2005

#### **ABSTRACT**

#### HYBRID CONTROL OF FLEXIBLE STRUCTURES

#### By

#### Shahin Sabokdast Nudehi

Active vibration control remains a topic of significant relevance and importance due to high performance demands of certain space structures as well as growing interest in the development of terrestrial structures using feedback control. This thesis presents two new approaches, to control system design for flexible structures. In the first approach, piezoelectric transducers are continually switched between actuator and sensor modes to enhance controllability and observability of the system. This approach can potentially reduce the number of piezoelectric transducers and associated hardware by 50%. In the second approach, piezoelectric transducers are used as sensors to estimate modal displacements and cables are used for the purpose of actuation. It is shown that tension in cables can be applied and released to directly suppress vibration of structures or vary the stiffness of the structure which results in modal energy redistribution. By properly designing switching strategies for the cable tension, modal energy can be redistributed, and specifically energy associated with higher modes can be funneled to the lower modes. This enables vibration suppression using a simple controller that can potentially sidestep the spillover problem.

## TABLE OF CONTENTS

L	LIST OF FIGURES		V
1	Intr	roduction	1
	1.1	Motivation	1
	1.2	Literature review	2
		1.2.1 Flexible structures with piezoelectric transducers	2
		1.2.2 Flexible structures with end-force	3
		1.2.3 Switched systems	5
	1.3	Scope and content of the dissertation	7
2	Mat	thematical Preliminaries	9
	2.1	Piezoelectric materials and properties	9
	2.2	Asymmetric configuration of piezo transducer	10
	2.3	State space modelling of beams with piezoelectric transducers	13
		2.3.1 Beam dynamics	13
		2.3.2 State equation with piezoelectric actuator	15
		2.3.3 Output equation with piezoelectric sensor	17
	2.4	Beam dynamics in the presence of an end-force	19
3	Swi	tching Piezos between Actuator and Sensor Modes	21
	3.1	Background	21
	3.2	Effect of switching on controllability and observability	22
	3.3	Switching requirement for observer-based controller	25
	3.4	Vibration suppression in a flexible beam	29
	3.5	Simulation of observer-based control design	30
	3.6	Sub-optimal switching schedule	33
	3.7	Experimental verification	37
		3.7.1 Apparatus	37
		3.7.2 Results	40

4	Vib	oration Control of a Flexible Beam using an End Force	4
	4.1	Background	4
	4.2	Mathematical model of cantilever beam with end-force	4
	4.3	Rayleigh-Ritz approximation	4
	4.4	Preliminary feedback control design	5
	4.5	Modified control design	5
	4.6	Adding bias tension in the cable	5
	4.7	Experimental verification	6
		4.7.1 Hardware description	6
		4.7.2 The effect of bias tension on structural damping	6
		4.7.3 Observer design	6
		4.7.4 Results	6
5	Modal Disparity		
	5.1	Background	6
	<b>5.2</b>	Proof of concept	6
	5.3	Dynamic analysis	7
	5.4	Numerical example	7
	5.5	Modified switching strategy	7
	5.6	Experimental Results	8
6	Cor	nclusion	8
$\mathbf{B}^{\dagger}$	BLI	OGRAPHY	80

## LIST OF FIGURES

2.1	Piezoelectric asymmetric configuration and associated distribution	11
2.2	A pined-pined Beam instrumented with PZT transducers	14
2.3	Free body diagram of element $dx$ with an end load $\ldots \ldots$	19
3.1	Plot of state variables in Example 1 for (a) $x_f = (0, 0)^T$ and (b)	
	$x_f = (-1, -2)^T \dots \dots \dots \dots \dots$	25
3.2	A simply supported flexible beam with two piezoelectric elements	29
3.3	Third and fourth mode shapes of beam in Figure (3.2) and location of	
	PZT elements in relation to these mode shapes	30
3.4	Amplitude of vibration of the (a) first, (b) second, (c) third, and (d)	
	fourth modes of the beam with observer-based control design	32
3.5	Amplitude of vibration of the (a) first, (b) second, (c) third, and (d)	
	fourth modes of the beam with sub-optimal switching	36
3.6	Experimental test-rig	37
3.7	Schematic of switching between actuator and sensor modalities	41
3.8	Experimental results: Plot of $y_{pzt}$ with time for (a) uncontrolled sys-	
	tem, and controlled system with (b) fixed switching schedule, (c) vari-	
	able switching schedule, and (d) sub-optimal switching schedule	43
3.9	(a) An observer-based controller (b) a discontinuous and (c) a con-	
	tinuous controller obtained from using a fixed-time and variable-time	
	switching schedule	44
4.1	A flexible cantilever beam with an end force	46
4.2	Simulation of decay in modal amplitude $a_1$ due to structural damping,	
	(b), (c) decay in modal amplitudes $a_1$ and $a_2$ due to control in the	
	presence of structural damping, and (d) plot of the control action	54
4.3	Control design based on output filtering	56
4.4	Plot of modal amplitudes $a_1$ and $a_2$ , and the control action $u$ for the	
	modified control design when $\epsilon = 0. \dots \dots \dots \dots$	58
4.5	Control design based on bias tension and output filtering	59

4.6	Experimental setup	61
4.7	Free vibration: (a) in the absence of bias tension, and (b) in the pres-	
	ence of 20 N bias tension	65
4.8	Vibration suppression using active control	66
4.9	Vibration suppression using a one mode dynamic model results a)-spill	
	over problem b)- the role of low pass filter in reducing the effect of	
	spillover	67
5.1	cantilever beam mode shapes for $P = 0$ and $P = 40N \dots$	70
<b>5.2</b>	Concept of the modal disparity	73
5.3	plot of the modal amplitude for the described switching strategy in	
	Equation (5.20)	76
5.4	Modified switching strategy	78
5.5	Plot of the modal amplitude and the end-force in the presence of the	
	low pass filter in the loop	79
5.6	Plot of the modal amplitude and the end-force in the presence of the	
	low pass filter and first order controller in the loop	81

## CHAPTER 1

### Introduction

#### 1.1 Motivation

Active vibration control remains a topic of significant relevance and importance due to high performance demands of certain space structures as well as growing interest in the development of terrestrial structures using feedback control. The traditional approach in active control of these structures is based on a linear system model in modal coordinates and estimation and control of the significant modes of the system using piezoelectric actuators and sensors. The problem of vibration suppression in highly flexible structures, such as space structures, require a large number of sensors and actuators, and piezoelectric transducers are commonly used as dedicated sensors and actuators. The hardware associated with piezoelectric actuators and sensors, such as power amplifiers and data acquisition boards, add significantly to the weight and cost of the system and motivates the development of control systems that require fewer transducers. It also motivates the development of viable control strategies that will be more effective than those based on the traditional approach, such that it can meet the high performance demands of the structures.

This thesis presents two new approaches, to control system design for flexible structures. In the first approach, piezoelectric transducers are continually switched be-

tween actuator and sensor modes to enhance controllability and observability of the system. This approach can potentially reduce the number of piezoelectric transducers and associated hardware by 50%. In the second approach, piezoelectric transducers are used as sensors to estimate modal displacements and cables are used for the purpose of actuation. It is shown that tension in cables can be applied and released to directly suppress vibration of structures or vary the stiffness of the structure which results in modal energy redistribution. By properly designing switching strategies for the cable tension, modal energy can be redistributed, and specifically energy associated with higher modes can be funnelled to the lower modes. This enables vibration suppression using a simple controller that can potentially sidestep the spillover problem.

#### 1.2 Literature review

#### 1.2.1 Flexible structures with piezoelectric transducers

There have been extensive studies on the use of piezoelectric transducers in structural control. Some of the early work on piezoelectric elements was aimed at developing actuator and sensor mathematical models (1991 Alberts and Colvin [1]; 1995 Alberts, et. al [2]; 1996 Fuller, et. al, [3]; 1998 Clark, et. al [4]). These models have been effectively used in control of flexible structures, (1987 Rawley and de Luis [5]; 1990 Hagood, et. al [6]; 1991 Garcia, et. al [7], 1991 Lazarus et. al. [8]), for example. The transfer function of flexible structures often have a large number of lightly damped modes and feedback control problems for systems of this nature are difficult to handle (1994 Skelton [9]). The control design for such systems are based on a finite number of modes and the resulting closed-loop system is prone to instability due to spillover (1978 Balas, [10], [11]). One way to avoid spillover is to have

a collocated structure which guarantees closed-loop system stability despite model truncation (2001 Halim and Moheimani [12]). In order to achieve perfect collocation, Anderson, et. al 1992, [13] and Dosch, et. al. 1992, [14] proposed the "sensoriactuator" or "self-sensing actuator". In their approach, a capacitor with capacitance identical to the piezoelectric element is used to resolve the mechanical strain of the structure. Some of the drawbacks of self-sensing are crosstalk (2001 Holterman and de Vries [15]) and lack of stability robustness due to capacitance uncertainty (1994 Cole and Clark, [16]: 2000 Acrabelli and Tonoli, [17]: 2003 Moheimani, [18]). Although switching piezoelectric elements between actuator and sensor modes has not been proposed earlier, Demetriou 2001, [19] and Murugavel, 2002 [20] proposed switching piezoelectric actuators between active and dormant states for optimization of a cost functional and improvement of closed-loop response. In our approach, presented in Chapter 3, a piezoelectric element is used both as an actuator and sensor, but not simultaneously. This can potentially avoid the problems encountered in self-sensing. Besides, it results in reduction of hardware and consequently reduction of cost and weight of the control system.

For flexible structures, an alternative way to reduce control system hardware is to use cables for vibration suppression. In Chapter 4, we show that a cable can be used to apply an end-force on a cantilever beam, and it can be switched on and off by a controller to suppress vibration.

#### 1.2.2 Flexible structures with end-force

To the best of our knowledge, there has been no work reported in the literature on vibration control of flexible structures using end forces. However, the dynamics of structural elements, such as beams and plates have been investigated under the application of end forces (e.g., 1963 Boltin, [21]; 1971 Herrmann, [22]; 1989 Higuchi, [23]; 1992 Dowell [23]; 2002 Hodges, et. al. [24]; 2000 Langthjem and Sugiyama,

[25]; 1996 O'Reilly, et. al, [26]; 2000 Park and Kim, [27]; 1996 Zuo and Schreyer, [28]). Most of the these results are related to the flutter instabilities associated with follower forces, which are nonconservative in nature. In our studies in Chapter 4 and 5, we use a cable to apply a conservative end force in a cantiliver beam.

In the literature, cables have been primarily used for increasing the stiffness of lightweight structures but there has been few studies on their use for vibration control. Achkire and Preumont (1996, [29]) investigated multiple control strategies for control of cable-stayed bridges and Preumont and Bossens (2000, [30]) used tendons to introduce active damping in truss structures. Skidmore and Hallauer (1985, [31]) demonstrated active damping in a beam-cable structure and Magana, et. al (1997, [32]) proposed a nonlinear control design to reduce vibartion introduced by external disturbances. In contrast of these approaches, Thomson et. al. (1995, [33]) proposed a passive method to significantly increase structural damping. They used shape memory alloy wires to constrain the motion of a beam and experimentally demonstrated that damping increases significantly when the wires are cyclically stressed with their pseudoelastic hysteresis loop.

In our approach, we do not restrict our control design to active damping. We use a cable to apply an end-force on a cantilever beam and demonstrate two different approaches for vibration control. The tension in the cable is switched on and off for direct vibration suppression of all the modes of the system and this approach is presented in Chapter 4. In Chapter 5, cable tension is switched to transfer energy from the higher modes to the lower modes of the system, which enables a simpler control system design. In both Chapters 4 and 5, the stability of the system is taken into consideration while designing switching strategies for cable tension. In the next section, we present a concise literature review of switched systems which has been a topic of considerable interest over the last decade.

#### 1.2.3 Switched systems

A switched systems consists of two or more continuous subsystems and a rule that orchestrate switching between them (1999 Liberzon and Morse [34]). In most control systems, switching between different subsystems occur because of changing dynamics or operating conditions of the plant, or change in the control law invoked for enhanced performance of the system. In Chapter 3, we propose switching piezoelectric transducers between actuator and sensor modes to enhance the controllability and observability of the system. The switching strategies developed in Chapters 4 and 5 are aimed at developing new control methodologies for flexible structures.

For switched systems, stability is an important consideration since the switching can introduce instability even when the individual subsystems are stable. Some of the important concepts in stability, such as "dwell time", and "common Lyapunov function" were proposed by [34]. Other approaches to the study of stability include the Lie-algebraic approach for linear systems (1999 Liberzon, Hespanha and Morse, [35]; 2001 Agrachev and Liberzon, [36]), extension of the invariance principle (2001, [37]), and the approach based on the Lyapunov functions and linear matrix inequalities (2000 DeCarlo, et. al, [38]). In our study in Chapter 3, where time interval between switchings is fixed, the issue of stability is addressed by designing stable subsystems and choosing the switching intervals to greater than the dwell time.

Some of the recent work on switched linear systems have addressed the issues of reachability and controllability. Ge, et. al (2002, [39]) and Zhenyu (2002, [40]) investigated controllability and observability of systems for pre-assigned switching sequences and Egerstedt (2002, [41]) investigated the complicity of the reachability problem between two given states for fixed number of switchings. In Chapter 4, we present observer-based control designs for a flexible beam in which controllability is guaranteed when all the piezoelectric transducers are used as actuators and observability is guaranteed

when all of them are used as sensors.

A part of our study in Chapter 3 is related to designing optimal switching sequences and intervals. Some of the early work on optimization of switched systems (1995 Branicky and Mitter, [42]; 1998 Branicky, et. al., [43]) used the maximum principle and dynamic programming to address general problems. In recent years, the focus has moved to specific switched systems. For example, Xu and Antsaklis (2002, [44]) addressed the problem of determining optimal switching instants for linear switched systems with fixed number of switchings and pre-specified sequence of autonomous subsystems. The total time was assumed to be finite in their approach but the infinite time horizon problem was investigated by Giua, et.al (2001, [45]). They assumed a quadratic performance index and considered discontinuities after switchings. The optimal control problem for switched linear systems with a known switching sequence and fixed switching intervals was addressed by Xu and Antsaklis (2002, [46]). They also addressed the more general problem of determining both optimal switching instants and optimal inputs for fixed number of switchings and pre-specified sequence of subsystems (2002 Xu and Antsaklis, [47]).

Most of the results on optimal control of switched systems provide open loop solutions. In contrast, Bemporad et. al (2002, [48]) obtained a solution to the problem of switching between finite number of autonomous subsystems based on state feedback. The time horizon was assumed to be infinite but Giua, et.al (2002, [49]) addressed the fixed final time problem. For both the problems, the number of switchings were assumed to be fixed but the sequence of subsystems were assumed not assigned apriori. The approach adopted in both cases applies well to two-dimensional systems but poses significant computational challenges for problems of higher dimensions. Furthermore, the approach is based on complete state information. The optimal control problem, where complete state information is not available and output variable description switches along with state variable description, has been investigated only by

a few researchers, such as Rantzer and Johansson (2000,[50]). The focus of this work, however, is to analyze the performance of the optimal control system and generalize concepts such as Grammians and LQR using the framework of piecewise quadratic Lyapunov functions.

#### 1.3 Scope and content of the dissertation

This thesis is organized as follows. In chapter 2, we present some background material that includes mathematical modelling of piezoelectric transducers. The state space model of an Euler-Bernoulli beam is derived for both cases where actuation is provided by a piezoelectric transducer and a cable providing an end force. These models are used in Chapters 3, 4 and 5 to design controllers for our flexible beam.

Chapter 3 starts with a discussion of the effect of switching on controllability and observability of linear time-variant systems. The requirement for observer-based control design, in terms of the number of switchings, is presented next. We establish the merit of introducing under-actuation and under-sensing with the objective of reducing the total number of piezoelectric transducers and associated hardware needed for vibration control. The feasibility of switching the piezoelectric transducers between actuator and sensor modalities was demonstrated by simulations as well as experiments.

In chapter 4, we study the dynamics of a cantilever beam with a buckling-type end force and derive its mathematical model for the purpose of feedback control design. Following that, we design a preliminary feedback control strategy for vibration suppression and demonstrate its efficiency through numerical simulations. We modify our control design to meet actuator bandwidth limitations and provide both simulation and experimental results based on the modified control design.

In Chapter 5, we introduce the concept of modal disparity. Modal disparity is a mea-

sure of the difference between modes in two stiffness states and can be exploited to gain control authority over the significant flexible modes of a system using a low dimensional state space model. Although stiffness variation in a structure can be achieved in many ways, we used cables to apply an end force for the cantilever beam problem. The control methodology relies on variation in stiffness of the beam to achieve modal energy redistribution, from higher modes to the lower modes, and dissipating the energy associated with the lower modes. Since the lower modes are only estimated and controlled, this approach has the potential to sidestep spillover problem. We present an analytical framework for control design exploiting the concept of modal disparity and verify the results through simulations and preliminary experiments. Chapter 6, provides concluding remarks and directions for future research.

## CHAPTER 2

## Mathematical Preliminaries

#### 2.1 Piezoelectric materials and properties

The piezoelectric effect was first discovered in 1880 by Pierre and Jacques Curie who demonstrated that when a stress field was applied to certain crystalline materials an electric charge was produced on the material surface [3]. It was subsequently demonstrated that the converse effect is also true; when an electric field is applied to a piezoelectric material it changes its size and shape. This effect is due to the electric dipoles of the material that spontaneously align themselves with the electric field. Due to the stiffness of the material, piezoelectric elements generate relatively large forces when their expansion is constrained. The relationship between applied forces and the resultant responses of piezoelectric materials depend upon a number of parameters, such as the material properties, size and shape, and direction in which forces or electrical fields are applied. The constitutive equations for a linear piezoelectric material, when the applied electric field and the generated stress are not very large, can be written as

$$\varepsilon^{i} = S_{ij}^{E} \sigma_{j} + d_{mi} E_{m}, \qquad (2.1)$$

$$D_m = d_{mi}\sigma_i + \xi_{ik}E_k, (2.2)$$

where the indices i, j = 1, 2, ..., 6 and m, k = 1, 2, 3 refer to different directions within the material coordinate system. In Equation (2.1)  $\varepsilon$ ,  $\sigma$ , D and E are the strain, stress, electrical displacement (charge per unit area) and the electric field (volts per unit length), respectively. In addition,  $S^E$ , d and  $\xi$  are the elastic compliance (the inverse of elastic modulus), piezoelectric strain constant, and permittivity of the material, respectively. For many structural applications, certain stress and strain terms in Equation (2.1) are negligible and in these cases the constitutive equations reduce to scalar equations. An example of such a structure is a flexible beam with a laminated piezoelectric. For this application, Equation (2.1) boils down to two scalar equations

$$\varepsilon^1 = \frac{1}{E_{pe}} \sigma_1 + d_{31} E_3, \tag{2.3a}$$

$$D_3 = d_{31}\sigma_1 + \xi_{33}E_3,\tag{2.3b}$$

In the absence of stress, Equation (2.3) can be simplified to

$$\varepsilon^1 = \frac{d_{31}V}{h_a} \tag{2.4}$$

where,  $d_{31}$ , the *piezoelectric strain constant*, is equal to the ratio of the developed free strain to the applied electric field  $E = V/h_a$ . In this equation V is the input voltage to the piezoelectric and  $h_a$  is the element thickness, as shown in Figure (2.1).

### 2.2 Asymmetric configuration of piezo transducer

One common form of arrangement of a piezoelectric actuator is the asymmetric configuration shown in Figure (2.1). In this arrangement, the actuator is bonded to the surface of the structure and when a voltage is applied across the electrodes (in direction of polarization) the actuator induces surface strains to the beam. It is assumed

that the beam is covered by a layer of thin piezoelectric material of thickness  $h_a$  (see Figure 2.1) which is perfectly bonded to the beam and produces a strain in the x direction only. When a voltage is applied across the bonded piezoelectric element it will attempt to expand but will be constrained due to stiffness of the beam. Due to symmetric nature of the load, the beam will both bend and stretch, leading to an asymmetric strain distribution as shown in Figure (2.1). In this figure, the origin of the z axis lies at the center of the beam. In the linear region, the strain distribution can be written as [3]

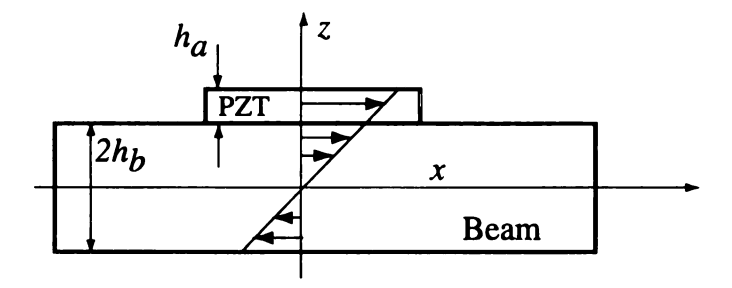


Figure 2.1. Piezoelectric asymmetric configuration and associated distribution

$$\varepsilon(z) = Cz + \varepsilon_0 \tag{2.5}$$

where C is the slope and  $\varepsilon_0$  is the z intercept. Equation (2.5) can be decomposed into the sum of an antisymmetric distribution Cz (i.e. flexural component) about the center of the beam and a uniform strain distribution  $\varepsilon_0$  (i.e longitudinal component) as shown in Figure (2.1). Using the strain distribution of Figure (2.1) and Hook's law, the stress distribution within the beam can be written as

$$\sigma_b(z) = E_b(Cz + \varepsilon_0) \tag{2.6}$$

where  $E_b$  is the Young's modules of the beam.

The stress distribution within the piezoelectric actuator,  $\sigma_{pe}(z)$ , is a function of the unconstrained actuator strain, the Young's modules of the material,  $E_{pe}$ , and the strain distribution shown in Figure 2.1. Mathematically it can be expressed as follows

$$\sigma_{pe}(z) = E_{pe}(Cz + \varepsilon_0 - \varepsilon_{pe}) \tag{2.7}$$

Applying force and moment equilibrium conditions about the center of the beam at the origin of the x axis, we get

$$\int_0^{h_b} \sigma_{pe}(z)dz + \int_{h_b}^{h_b + h_a} \sigma_{pe}(z)dz = 0$$
 (2.8)

$$\int_0^{h_b} \sigma_{pe}(z)zdz + \int_{h_b}^{h_b + h_a} \sigma_{pe}(z)zdz = 0$$
 (2.9)

where  $h_b$  is the half-thickness of the beam. In order to solve for the unknowns C and  $\varepsilon_0$ , we integrate Equation (2.8) to get

$$\varepsilon_0 = K^L \varepsilon_{pe} \tag{2.10}$$

where  $K^L$  is the material geometric constant, given by the expression [3]

$$K^{L} = \frac{E_{pe}h_{a}(8E_{b}h_{b}^{3} + E_{pe}h_{a}^{3})}{16E_{b}^{2}h_{b}^{4} + E_{b}E_{pe}(32h_{b}^{3}h_{a} + 24h_{b}^{2}h_{a}^{2} + 8h_{b}h_{a}^{3}) + E_{pe}^{2}h_{a}^{4}}$$
(2.11)

and C is the slope, given by the expression

$$C = K^f \varepsilon_{pe} \tag{2.12}$$

where  $K^f$  is a constant [3] given by

$$K^{f} = \frac{12E_{b}E_{pe}h_{b}h_{a}(2h_{b} + h_{a})}{16E_{b}^{2}h_{b}^{4} + E_{b}E_{pe}(32h_{b}^{3}h_{a} + 24h_{b}^{2}h_{a}^{2} + 8h_{b}h_{a}^{3}) + E_{pe}^{2}h_{a}^{4}}$$
(2.13)

Equations (2.12 and 2.13) imply that the induced moment distribution in the beam beneath the actuator,  $m_x$ , is

$$m_x(x) = E_b I_b K^f \varepsilon_{pe} (2.14)$$

$$= \frac{E_b I_b K^f d_{31}}{h_a} V (2.15)$$

$$= K_a V \tag{2.16}$$

where  $E_b$  and  $I_b$  are the elasticity and moment inertia of the beam respectively. The response of the beam to the asymmetric actuator, as shown in Figure 2.1, consists of a moment distribution  $m_x$  proportional to the excitation voltage V, specified by Equation (2.16), and a longitudinal strain distribution  $\varepsilon(z)$ , specified by Equation (2.5). The longitudinal strain is also proportional to the voltage and can be ignored in comparison to the flexural component.

## 2.3 State space modelling of beams with piezoelectric transducers

#### 2.3.1 Beam dynamics

In this section we derive the equation of a flexible beam governing the dynamics of a flexible beam using a piezoelectric actuator. In this derivation, the effects of shear deformation and rotary inertia are not considered and it is assumed all the displacements are small (Euler-Bernoulli beam). In Figure (2.2) the lateral vibration of the

beam in the xy plane is shown wherein a piezoelectric actuator and a piezoelectric sensor patch are bonded between locations  $x_1$  and  $x_2$ , and  $x_3$  and  $x_4$ , respectively. Consider a free-body of an element of the beam shown in Figure (2.2). From Newton's

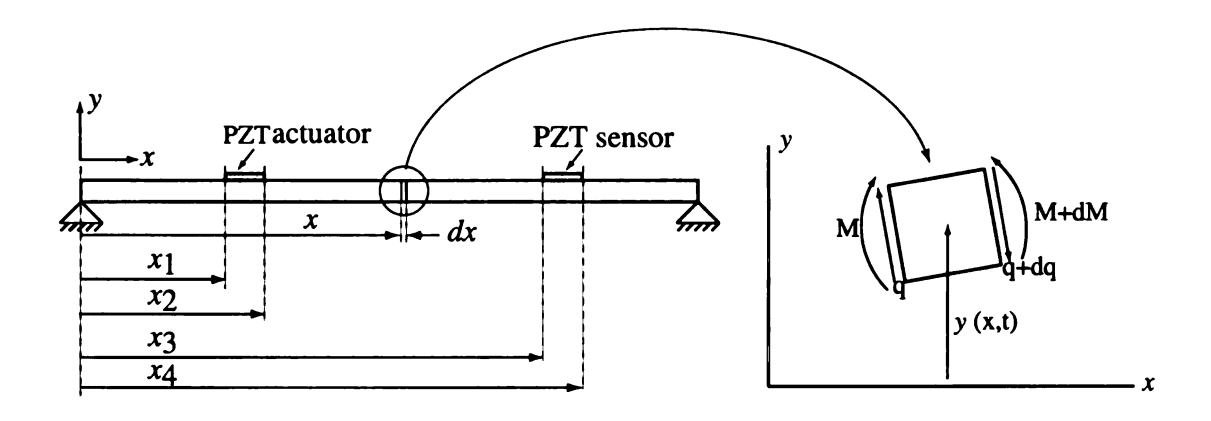


Figure 2.2. A pined-pined Beam instrumented with PZT transducers

second law, the dynamic force in the lateral direction is [3]

$$m\frac{\partial^2 y(x,t)}{\partial t^2}dx = -(q + \frac{\partial q}{\partial x}dx) + q$$
 (2.17)

or

$$m\frac{\partial^2 y(x,t)}{\partial t^2} = -\frac{\partial q}{\partial x} \tag{2.18}$$

where m is mass per unit length of the beam and q is the shear force. Summing the moments M about any point on the right face of the element yields

$$M = \frac{\partial q}{\partial x} \tag{2.19}$$

Where M is comprised of two parts, namely, the distributed moment produced by the piezoelectric actuator (equal to  $K_aV$  between  $x_1$  and  $x_2$  and zero anywhere else),

and the moment due to beam curvature. Thus

$$M = K_a V(Heaviside(x - x_1) - Heaviside(x - x_2)) + E_b I_b \frac{\partial^2 y(x, t)}{\partial t^2}$$
 (2.20)

By combining Equations (2.18 to 2.20) we get the following equation for lateral vibration of the beam

$$E_b I_b \frac{\partial^4 y(x,t)}{\partial x^4} + m \frac{\partial^2 y(x,t)}{\partial t^2} = K_a V(\delta'(x-x_2) - \delta'(x-x_1))$$
 (2.21)

where  $\delta'(.)$  is the derivative of the Dirac function with respect to x.

#### 2.3.2 State equation with piezoelectric actuator

In this section a state-space model of Equation (2.21) is presented from [51]. In this representation the input to the system is the voltage V applied to the piezoelectric actuator. we assume that the effects of the laminated piezoelectric actuator on the mode shapes is negligible, which is a valid assumption if the dimensions of the piezoelectric are small compared with those of the beam.

From the theory of vibrations, we know that the lateral displacement of a beam can be written in modal coordinates as follows

$$y(x,t) = \sum_{i=1}^{\infty} \phi_i(x)\eta_i(t)$$
 (2.22)

where  $\phi_i(x)$  are the normalized orthogonal mode shapes and the  $\eta_i(t)$  are the modal amplitudes. Substituting Equation (2.22) into Equation (2.21) and projecting on to the  $i^{th}$  mode yields the  $i^{th}$  decoupled modal equation

$$m\ddot{\eta}_i(t) + E_h I_h \psi_i \eta_i(t) = [\phi'(x - x_2) - \phi'(x - x_1)] K_a V(t)$$
 (2.23)

where,  $\psi_i$  is given by

$$\psi_i = \int_0^{L_b} \phi_i(x) \phi_i''''(x) \tag{2.24}$$

and where,  $L_b$  is the beam length. If we define

$$\omega_i^2 \triangleq \frac{E_b I_b \psi_i}{m}$$

$$B_i \triangleq \frac{1}{m} [\phi'(x - x_2) - \phi'(x - x_1)] K$$

$$(2.25)$$

$$B_i \triangleq \frac{1}{m} [\phi'(x - x_2) - \phi'(x - x_1)]K$$
 (2.26)

Equation (2.23) can be written as

$$\ddot{\eta_i}(t) + \omega_i^2 \eta_i(t) = B_i V(t) \tag{2.27}$$

It is clear from this equation that the  $i_{th}$  mode is controllable if and only if  $B_i$  is nonzero. If we truncate our representation to n modes, meaning that we are interested in the first n modes of oscillation only, Equation (2.27) can be written as

$$\dot{z}(t) = \bar{A}z(t) + \bar{B}V(t) \tag{2.28}$$

where

$$\bar{A} \triangleq \begin{bmatrix} 0_n & I_n \\ -\Omega^2 & 0_n \end{bmatrix} \tag{2.30}$$

$$\bar{B} \triangleq \begin{bmatrix}
0_n \\
B_1 \\
B_2 \\
\vdots \\
B_n
\end{bmatrix}$$
(2.31)

where  $\Omega \triangleq diag\{\omega_1, ..., \omega_n\}$ , and  $0_n$  and  $I_n$  are zero and identity matrices, respectively, of dimension  $n \times n$ . In this derivation, structural damping of the beam is not taken into the consideration. One might approximate the effect of structural damping by viscous damping through modifying the  $\bar{A}$  matrix as follows

$$\bar{A} \triangleq \begin{bmatrix} 0_n & I_n \\ -\Omega^2 & -2\zeta\Omega \end{bmatrix}$$
 (2.32)

where  $\zeta$  is the viscous damping coefficient.

#### 2.3.3 Output equation with piezoelectric sensor

For a piezoelectric material, the ratio of the strain in the material to the charge density is constant and is denoted by

$$g_{31} = \frac{\text{Strain Developed}}{\text{Applied Charge Density}}$$
 (2.33)

The incremental charge dQ generated on an infinitesimal area of the piezoelectric (assuming the width of the piezoelectric to be equal to the width of the beam, b) is therefore

$$dQ = \frac{\partial^2 y(x,t)/\partial x^2}{q_{31}} h_b b dx \qquad (2.34)$$

where b and  $2h_b$  are the width and thickness of the beam, respectively. Equation (2.34) can be integrated over length of the beam covered by the piezoelectric sensor to yield

the expression for the output voltage,  $V_s$ ,

$$V_s(t) = \frac{b h_b}{g_{31} C_p} (y'(x_4, t) - y'(x_3, t))$$
 (2.35)

$$V_s(t) \triangleq K_s(y'(x_4, t) - y'(x_3, t))$$
 (2.36)

where  $C_p$  is the capacitance, and  $x_3$  and  $x_4$  are the start and the end locations of the piezoelectric sensor on the beam (see Figure (2.2)). Substituting Equation (2.22) into Equation (2.36) yields

$$V_s(t) = K_s \sum_{i=1}^{\infty} \eta_i(t) [\phi_i'(x_4) - \phi_i'(x_3)]$$
 (2.37)

For an n mode approximation, we have

$$V_s(t) = K_s \sum_{i=1}^n \eta_i(t) [\phi_i'(x_4) - \phi_i'(x_3)]$$
 (2.38)

Byt defining  $C_i$  as

$$C_i = K_s[\phi_i'(x_4) - \phi_i'(x_3)] \tag{2.39}$$

we get

$$V_s(t) = C_i z(t) (2.40)$$

It should be noted that the  $i^{th}$  mode is observable if and only if  $C_i$  is nonzero.

Equation (2.28) together with Equation (2.40) provide a state space representation of the dynamics of an Euler-Bernoulli beam with a piezoelectric actuator and a piezoelectric sensor.

#### 2.4 Beam dynamics in the presence of an end-force

In this section we present the mathematical model of a flexible beam in the presence of an end-load. The nature of the end-load can be either conservative such as an axial force (buckling force) or non-conservative such as a follower force, or it can be a combination of both. Consider the free-body diagram of an element dx along the length of beam shown in Figure (2.3). The force P reflects the end load and it is assumed to be constant for small deflections of the beam. Now, let m = mass/length,  $\theta = \partial y(x,t)/\partial x = \text{slope}$ , and q = shear force, shown in Figure (2.3).

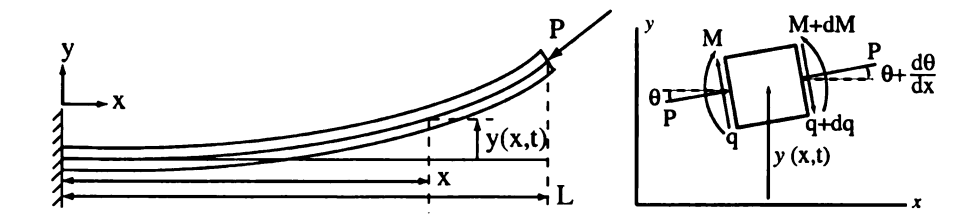


Figure 2.3. Free body diagram of element dx with an end load

From Newton's second law, we have

$$m\frac{\partial^2 y(x,t)}{\partial t^2}dx = -(q + \frac{\partial q}{\partial x}dx) + q - P(\theta + \frac{\partial \theta}{\partial x}dx) + P\theta$$
 (2.41)

or

$$m\frac{\partial^2 y(x,t)}{\partial t^2} = -\frac{\partial q}{\partial x} - P(\frac{\partial^2 y(x,t)}{\partial x^2})$$
 (2.42)

Substituting Equation (2.18) in Equation (2.42) results in

$$E_b I_b \frac{\partial^4 y(x,t)}{\partial x^4} + m \frac{\partial^2 y(x,t)}{\partial t^2} + P \frac{\partial^2 y(x,t)}{\partial x^2} = 0$$
 (2.43)

which is the equation of the beam in the presence of the end load P. It should be noticed that the governing equation is independent of the type of the end load (axial, follower, etc.). The boundary conditions for these different cases, however, will be different. We will discuss the boundary conditions for our particular case in Chapters 4 and 5.

## CHAPTER 3

# Switching Piezos between Actuator and Sensor Modes

#### 3.1 Background

In the first part of this chapter we develop general results for gaining controllability and observability in under-actuated and under-sensed systems through switching. In our study, as different from the work in [52], [53], where controllability and observability for pre-assigned switching sequences is studied, we investigate the minimum number of switchings required to achieve controllability, observability, and to design controllers based on observers. In the second part of this chapter, we present a novel application of switching control for vibration suppression in flexible structures. We consider a flexible Euler-Bernoulli beam instrumented with PZTs for our simulation and experiments. The PZTs are attached to the beam such that the system is completely controllable when all of them are used as actuators and completely observable when all of them are used as sensors. The underlying objective is to switch piezo transducers between actuator and sensor modes and thereby reduce the number of transducers and associated hardware required for vibration suppression.

## 3.2 Effect of switching on controllability and observability

Consider a multi-input linear time-invariant system with the minimum number of inputs required for complete controllability. Now imagine a situation where all the inputs cannot be used at the same time, meaning that there are some inputs that can be used in the control loop (active) while the rest cannot be used (inactive). This system will not be completely controllable. If the roles of the active and inactive inputs are reversed, the new system will still lack complete controllability since it will have a set of inactive inputs. The time-varying system, comprised of the two time-invariant systems, with the inputs switching between their active and inactive modes will however be controllable. This is stated with the help of the following Theorem.

**Theorem 1:** Consider the linear time-varying system that switches between the two time-invariant systems

$$\dot{x} = Ax + B_1 u_1, \qquad \dot{x} = Ax + B_2 u_2, \qquad x(t_0) = x_0$$
 (3.1)

where  $x \in \mathbb{R}^n$  and  $\{A, [B_1, B_2]\}$  is completely controllable, but neither  $\{A, B_1\}$  nor  $\{A, B_2\}$  are completely controllable. The switched time-varying system is completely controllable on the interval  $[t_0, t_2]$  if and only if the number of switchings within the interval is one or greater.

**Proof:** To prove sufficiency, consider one switching at  $t = t_1$ ,  $t_0 < t_1 < t_2$ . Then, the controllability grammian can be written as

$$W(t_0, t_2) = \int_{t_0}^{t_1} \Phi(t_0, t) B_1 B_1^T \Phi^T(t_0, t) dt + \int_{t_1}^{t_2} \Phi(t_0, t) B_2 B_2^T \Phi^T(t_0, t) dt$$
 (3.2)

where  $\Phi(t_0, t)$  is the state transition matrix. We prove sufficiency, i.e. show that

the grammian is full-rank, by contradiction. If the grammian is rank deficient, we can find a vector  $x_a$ ,  $x_a \neq 0$ , such that  $x_a^T W(t_0, t_2) x_a = 0$ . This implies

$$x_a^T \Phi(t_0, t) B_1 = 0, \quad t_0 \le t < t_1$$
 (3.3a)

$$x_a^T \Phi(t_0, t) B_2 = 0, \quad t_1 \le t \le t_2$$
 (3.3b)

Considering the time-invariant nature of the individual systems in (3.1), we can claim

$$x_a^T[B_1, AB_1, A^2B_1, \cdots A^{n-1}B_1] = 0, \qquad x_a^T[B_2, AB_2, A^2B_2, \cdots A^{n-1}B_2] = 0$$

$$(3.4)$$

which can be written as

$$x_a^T[[B_1, B_2], A[B_1, B_2], \cdots A^{n-1}[B_1, B_2]] = 0$$
 (3.5)

The above equation violates the assumption that  $[A, [B_1, B_2]]$  is controllable and this proves that the grammian is full-rank, or the time-varying system is controllable. To prove necessity, we simply show the grammian to have rank deficiency for  $t_1 > t_2$ , which corresponds to the case of no switching.  $\diamond \diamond \diamond$ 

The result in Theorem 1 can also be deduced from Theorem 2 in [52]. A simple example is presented next to illustrate the result in Theorem 1.

**Example 1:** We assume the two time-invariant systems in Theorem 1 to have the description

$$A \triangleq \begin{pmatrix} 1 & 0 \\ 0 & 2 \end{pmatrix}, \qquad B_1 \triangleq \begin{pmatrix} 1 \\ 0 \end{pmatrix}, \qquad B_2 \triangleq \begin{pmatrix} 0 \\ 1 \end{pmatrix}$$
 (3.6)

Clearly,  $\{A, B_1\}$  and  $\{A, B_2\}$  are not completely controllable, whereas  $\{A, [B_1, B_2]\}$  is completely controllable. For  $t_0 = 0.0$ ,  $t_1 = 0.5$ ,  $t_2 = 1.0$ , and initial system

description  $\dot{x} = Ax + B_1u_1$ , the state transition matrix and controllability grammian are described by the relations

$$\Phi(0,t) = \begin{bmatrix} e^{-t} & 0 \\ 0 & e^{-2t} \end{bmatrix}, \qquad W(0,1) = \begin{bmatrix} -(e^{-1}-1)/2 & 0 \\ 0 & -(e^{-4}-e^{-2})/4 \end{bmatrix}$$
(3.7)

To converge the system states to  $x=x_f$  at  $t_2=1.0$ , we designed a controller for the time-varying system as follows [54]

$$u(t) = B^{T}(t)\Phi^{T}(0,t)W^{-1}(0,1)\left\{-x_0 + \Phi(0,1)x_f\right\}, \quad 0.0 \le t \le 1.0$$
 (3.8)

where

$$B(t) = \begin{cases} \begin{pmatrix} 1 & 0 \\ 0 & 0 \end{pmatrix} & \text{for } 0 \le t < 0.5 \\ \\ \begin{pmatrix} 0 & 0 \\ 0 & 1 \end{pmatrix} & \text{for } 0.5 \le t < 1.0 \end{cases}$$
(3.9)

The simulation results for  $x_f = (0,0)^T$  and  $x_f = (-1,-2)^T$  are shown in Figure (3.1), respectively. The results show that all the states are converged to their desired values. It should be noted from Figure (3.1a) that  $x_1$  is converged to zero at t = 0.5 since  $x_1$  is uncontrollable thereafter. For  $0.5 \le t \le 1.0$ ,  $x_1$  remains at zero since  $x_1 = 0$  is an equilibrium point. In the case of Figure (3.1b),  $x_1$  is converged to an intermediate value at t = 0.5. Starting at this intermediate value,  $x_1$  converges to its desired value of -1 over the interval  $0.5 \le t \le 1.0$ , simply by virtue of being unstable. In both cases, the state  $x_2$  is uncontrollable during the first interval but is converged to its desired value by proper choice of input  $u_2$  over the interval  $0.5 \le t \le 1.0$ .

Since observability is a dual property of controllability, we extend the result in

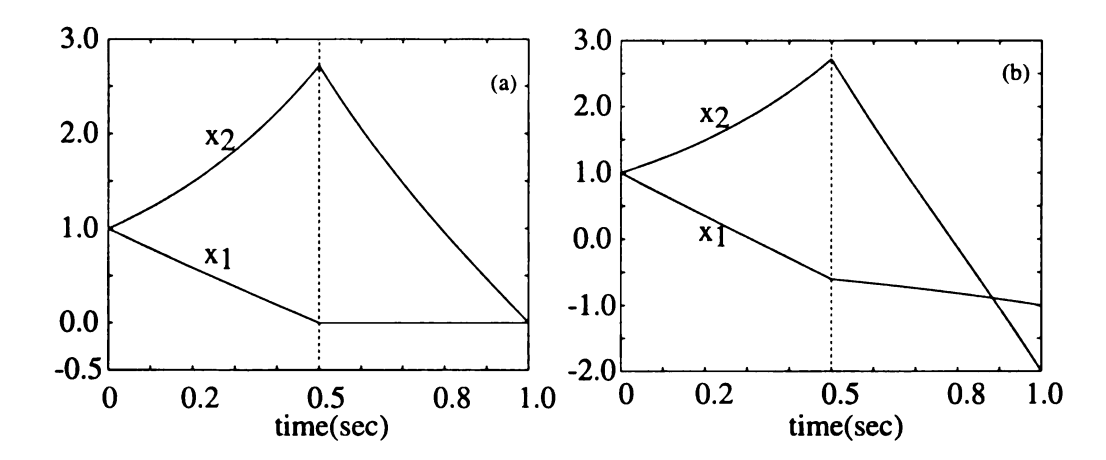


Figure 3.1. Plot of state variables in Example 1 for (a)  $x_f = (0, 0)^T$  and (b)  $x_f = (-1, -2)^T$ 

Theorem 1 to the problem of state estimation using Theorem 2, stated next.

**Theorem 2:** Consider the linear system  $\dot{x} = Ax + Bu$ , whose output is time-varying and switches between the relations

$$y_1 = C_1 x, y_2 = C_2 x (3.10)$$

where  $\{A,C\}$  is observable for  $C=[C_1^T,C_2^T]^T$ , but  $\{A,C_1\}$  and  $\{A,C_2\}$  are not observable. The switched system is observable on an interval if and only if the number of switchings within the interval is one or greater.

**Proof:** The proof is very similar to the proof of Theorem 1.  $\diamond \diamond \diamond$ 

## 3.3 Switching requirement for observer-based controller

The controller used in Example 1, given by the expression in Equation (3.8), assumes knowledge of the initial state  $x_0$ . If the initial state is unknown, it has to be first

estimated and if Equation (3.10) represents the output description of the system, one switching will be required for state estimation. This follows from Theorem 2 and motivates the next theorem on observer-based control design.

**Theorem 3:** (Observer-based Controller) Consider the linear time-varying system that switches between the two time-invariant descriptions

$$\Sigma_1: \dot{x} = Ax + B_1 u_1, \quad y_1 = C_1 x$$
 (3.11a)

$$\Sigma_2: \dot{x} = Ax + B_2 u_2, \quad y_2 = C_2 x$$
 (3.11b)

If  $x=(x_1^T,\,x_2^T,\,x_3^T)^T$ , where  $x_1\in R^p$  is controllable and observable (CO) for both  $\Sigma_1$  and  $\Sigma_2,\,x_2\in R^q,\,q\neq 0$ , is controllable but unobservable  $(C\bar{O})$  for  $\Sigma_1$  and uncontrollable but observable  $(\bar{C}O)$  for  $\Sigma_2$ , and  $x_3\in R^r,\,r\neq 0$ , is  $\bar{C}O$  for  $\Sigma_1$  and  $C\bar{O}$  for  $\Sigma_2$ , then

- (i)  $\{A, B_1\}$ ,  $\{A, B_2\}$  are not completely controllable but  $\{A, [B_1, B_2]\}$  is completely controllable.
- (ii)  $\{A, C_1\}$ ,  $\{A, C_2\}$  are not completely observable but  $\{A, [C_1^T, C_2^T]^T\}$  is completely observable.
- (iii) All the states of the switched system can be steered to the origin in finite time using estimated states if and only if the number of switchings is two or more.

**Proof:** Since  $r \neq 0$ ,  $\{A, B_1\}$  is not completely controllable. Similarly,  $\{A, B_2\}$  is not completely controllable since  $q \neq 0$ . The states  $x_1$  and  $x_2$  are controllable with input matrix  $B_1$  whereas states  $x_1$  and  $x_3$  are controllable with input matrix  $B_2$ . Therefore, all the states,  $x_1, x_2, x_3$ , are controllable with input matrix  $[B_1, B_2]$ . This completes the proof of (i). The proof of (ii) is very similar to that of (i) and is skipped. We prove (iii) next, as follows:

Sufficiency: Let the initial time be  $t_0$  and the initial state be  $x_0 = x(t_0)$ . For the purpose of convenience, we define  $u = \{u_1^T, u_2^T\}^T, y = \{y_1^T, y_2^T\}^T$ , and without loss of generality we assume the initial system description to be  $\Sigma_1$ . To prove sufficiency for two switchings, we assume the switching instants to be  $t = t_1$  and  $t = t_2$ , the final time to be  $t_f$ , and  $t_{12}$  to be an intermediate time, all of which satisfy  $t_0 < t_1 <$  $t_{12} < t_2 < t_f$ . We now claim that the following observer-based control design moves all states of the switched system to the origin:

$$u(t) = \begin{cases} 0, & t_0 \le t < t_{12} \\ -B^T(t)\phi^T(t_{12}, t)W^{-1}(t_{12}, t_f)\phi(t_{12}, t_0)V^{-1}(t_0, t_{12}) \int\limits_{t_0}^{t_{12}} \phi^T(\tau, t_0)C^T(\tau)y(\tau)d\tau, & t_{12} \le t \le t_f \end{cases}$$

$$(3.12)$$

In the above equation, W(.,.) and V(.,.) are the controllability and observability grammians, respectively,  $\phi(.,.)$  is the state transition matrix, and B(t) and C(t) are defined as follows:

$$B(t) = \begin{cases} (B_1, 0), & \text{for } t_0 \le t < t_1 \\ (0, B_2), & \text{for } t_1 \le t < t_2 \\ (B_1, 0), & \text{for } t_2 \le t \le t_f \end{cases}$$

$$C(t) = \begin{cases} (C_1^T, 0)^T, & \text{for } t_0 \le t < t_1 \\ (0, C_2^T)^T, & \text{for } t_1 \le t < t_2 \\ (C_1^T, 0)^T, & \text{for } t_2 \le t \le t_f \end{cases}$$

$$(3.13a)$$

$$C(t) = \begin{cases} (C_1^T, 0)^T, & \text{for } t_0 \le t < t_1 \\ (0, C_2^T)^T, & \text{for } t_1 \le t < t_2 \\ (C_1^T, 0)^T, & \text{for } t_2 \le t \le t_f \end{cases}$$
(3.13b)

To prove our claim, we first note that y(t) = C(t)x(t) and  $y(t) = C(t)\phi(t,t_0)x_0$  on the interval  $t_0 \le t < t_{12}$  since u = 0 on this interval. From (ii) we know that the switched system in Equation (3.11) satisfies the conditions of Theorem 2. Furthermore, there is one switching in the interval  $[t_0, t_{12})$ . Therefore, the observability grammian

$$V(t_0, t_{12}) = \int_{t_0}^{t_{12}} \phi^T(\tau, t_0) C^T(\tau) C(\tau) \phi(\tau, t_0) d\tau$$
 (3.14)

is nonsingular and its inverse exists. Hence  $x(t_{12})$  can be estimated as follows

$$x(t_{12}) = \phi(t_{12}, t_0)x_0 \tag{3.15a}$$

$$= \phi(t_{12}, t_0)V^{-1}(t_0, t_{12})V(t_0, t_{12})x_0 \tag{3.15b}$$

$$= \phi(t_{12}, t_0) V^{-1}(t_0, t_{12}) \int_{t_0}^{t_{12}} \phi^T(\tau, t_0) C^T(\tau) C(\tau) \phi(\tau, t_0) x_0 d\tau (3.15c)$$

$$= \phi(t_{12}, t_0) V^{-1}(t_0, t_{12}) \int_{t_0}^{t_{12}} \phi^T(\tau, t_0) C^T(\tau) y(\tau) d\tau$$
 (3.15d)

Equation (3.15) is true since since u = 0 over the interval  $[t_0, t_{12})$ . Using this equation, our claim in Equation (3.12) can be simplified to the form

$$u = -B^{T}(t)\phi^{T}(t_{12}, t)W^{-1}(t_{12}, t_{f})x(t_{12}) \qquad t_{12} \le t \le t_{f}$$
(3.16)

From (i) we know that the switched system in Equation (3.11) satisfies the conditions of Theorem 1. Since there is one switching within the interval  $[t_{12}, t_f]$ , the controllability grammian  $W(t_{12}, t_f)$  is nonsingular and hence the control input given by Equation (3.16) moves the states from  $x(t_{12})$  at  $t = t_{12}$  to their final values  $x_f = 0$  at  $t = t_f$ . This can be easily deduced from Equation (3.8) in Example 1. The above proof can be easily modified to establish sufficiency when the number of switchings is greater than two.

Necessity: Let the initial and final times be  $t_0$  and  $t_f$ , respectively. We prove necessity by contradiction. Suppose all the states,  $x = \{x_1^T, x_2^T, x_3^T\}^T$ , can be steered to the origin at  $t = t_f$  after one switching at  $t = t_1$  ( $t_0 < t_1 < t_f$ ) using estimated states. Let the initial system description be  $\Sigma_1$  and it switches to  $\Sigma_2$  after the switching. Since  $q \neq 0$ ,  $x_2$  is the nonzero set of uncontrollable states of  $\Sigma_2$ . Since  $x_2$  is not controllable,  $x_2(t_f) = 0$ , and  $(t_f - t_1)$  is finite, we must have  $x_2(t) = 0$ ,  $\forall t \in [t_1, t_f]$ . Although  $x_2$  is controllable in  $\Sigma_1$ , it is not observable. Therefore, it cannot be steered to  $x_2(t_1) = 0$  from an arbitrary initial condition,

 $x_2(t_0)$ , in finite time. This contradicts our earlier claim that  $x_2(t_1) = 0$ . If the initial system description is  $\Sigma_2$  and it switches to  $\Sigma_1$  after the switching,  $x_3$  is the nonzero set of uncontrollable states of  $\Sigma_1$ , since  $r \neq 0$ . We can again prove by contradiction that it is not possible to steer  $x_3$ , and hence all the states, to the origin in finite time.  $\diamond \diamond \diamond$ 

In our discussion so far, we did not address the issue of stability. It is well known, [34] for example, that arbitrary switching between asymptotically stable systems can result in instability. For our observer-based control designs, we will avoid this problem by simply ensuring that the switching interval is greater than the dwell time [34].

### 3.4 Vibration suppression in a flexible beam

In this section we consider the problem of vibration suppression in the flexible beam shown in Figure (3.2). Our objective is to design an observer-based feedback controller that will suppress the vibration in the first four modes of the beam using the two PZT elements shown in the figure.

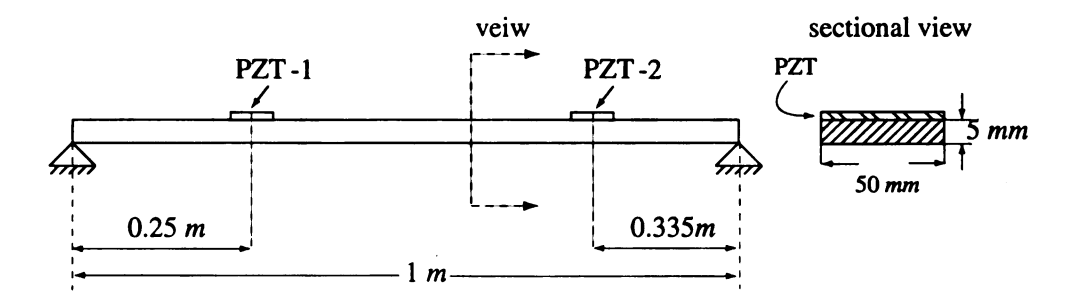


Figure 3.2. A simply supported flexible beam with two piezoelectric elements

In conformity with our discussion in Section 2, we define the linear time-invariant system  $(A, B_1, C_1)$  based on use of PZT-1 as the actuator and PZT-2 as the sensor, and the system  $(A, B_2, C_2)$  based on use of PZT-1 as the sensor and PZT-2 as the

actuator. For the goal of vibration suppression in the first four modes (n=4), it can be easily inferred from Figure (3.3) that the fourth mode is uncontrollable and the third mode is unobservable for  $(A, B_1, C_1)$  since PZT-1 lies at the node of the fourth mode and PZT-2 lies at the node of the third mode. For  $(A, B_2, C_2)$ , we can similarly conclude that the third mode is uncontrollable and the fourth mode is unobservable. In relation to our discussion in Section 3.2, we have p=4, q=2, and r=2 for both systems  $(A, B_1, C_1)$  and  $(A, B_2, C_2)$ . For example, the controllable and observable states corresponding to p=4 are comprised of the displacement and velocity of the first and second modes.

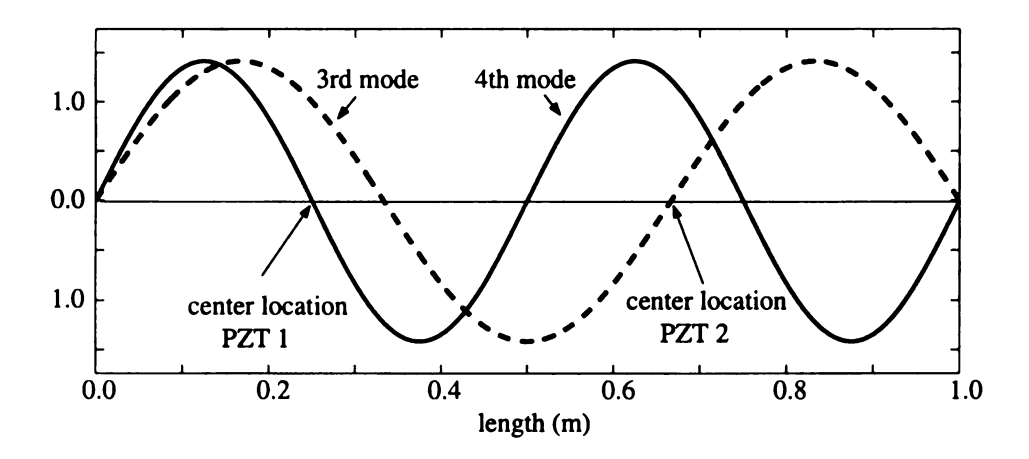


Figure 3.3. Third and fourth mode shapes of beam in Figure (3.2) and location of PZT elements in relation to these mode shapes

### 3.5 Simulation of observer-based control design

The two linear time-invariant systems  $(A, B_1, C_1)$  and  $(A, B_2, C_2)$ , discussed in Section 3.4, have the explicit form

$$\dot{x} = Ax + B_1 u_1, \qquad y_1 = C_1 x \tag{3.17a}$$

$$\dot{x} = Ax + B_2 u_2, \qquad y_2 = C_2 x \tag{3.17b}$$

where  $x \in \mathbb{R}^8$ , and  $u_1, u_2, y_1, y_2 \in \mathbb{R}$ . Using the beam dimensions in Figure (3.2),  $\zeta = 0.01$ , material properties of aluminum, and mathematical relations given in Chapter 2, the entries of the matrices A,  $B_1$ ,  $B_2$ ,  $C_1$ , and  $C_2$ , defined in Equations (3.17), were computed as follows

$$A = \begin{bmatrix} 0_n & I_n \\ -\Omega^2 & -2\zeta\Omega \end{bmatrix}$$
 (3.18a)

$$\Omega^2 = \pi^4 \operatorname{diag}(58.3, 933.3, 4725, 14933.3)$$
 (3.18b)

$$B_1 = [O_{1\times4}, -0.006, -0.032, -0.044, 0.000]^T$$
 (3.18c)

$$B_2 = [O_{1\times4}, -0.004, -0.016, 0.000, 0.058]^T$$
 (3.18d)

$$C_1 = [-0.606, 2.369, 0.000, -8.659, O_{1\times4}] \times 10^5$$
 (3.18e)

$$C_2 = [-0.910, -4.757, -6.592, 0.000, O_{1\times4}] \times 10^5$$
 (3.18f)

It is clear from the zero entries of  $B_1$  and  $C_1$  in Equations (3.18) that the fourth mode is not controllable and the third mode is not observable for  $(A, B_1, C_1)$ . Similarly, the third mode is not controllable and the fourth mode is not observable for  $(A, B_2, C_2)$ . For both systems, we designed observer-based controllers as follows

$$u_1 = -K_1 \hat{x} \qquad \dot{\hat{x}} = A\hat{x} + B_1 u_1 + L_1 (y_1 - C_1 \hat{x})$$
 (3.19a)

$$u_2 = -K_2 \hat{x}$$
  $\dot{\hat{x}} = A\hat{x} + B_2 u_2 + L_2 (y_2 - C_2 \hat{x})$  (3.19b)

where the matrices of controller and observer gains,  $K_1$ ,  $K_2$ ,  $L_1$ ,  $L_2$  were designed using standard pole-placement techniques. Although these matrices are not shown here for the sake of brevity, it should be noted that the entries of  $K_1$  and  $K_2$  ( $L_1$  and  $L_2$ ), that correspond to the uncontrollable (unobservable) states, are zero. Our

simulation results, for initial conditions are shown in Figure (3.4).

$$x(0) = (0.2, -0.4, 0.2, 0.2, 0.08, 0.0, -0.2, -0.4)^T, \ \widehat{x}(0) = (O_{1\times4}, O_{1\times4})^T \ (3.20)$$

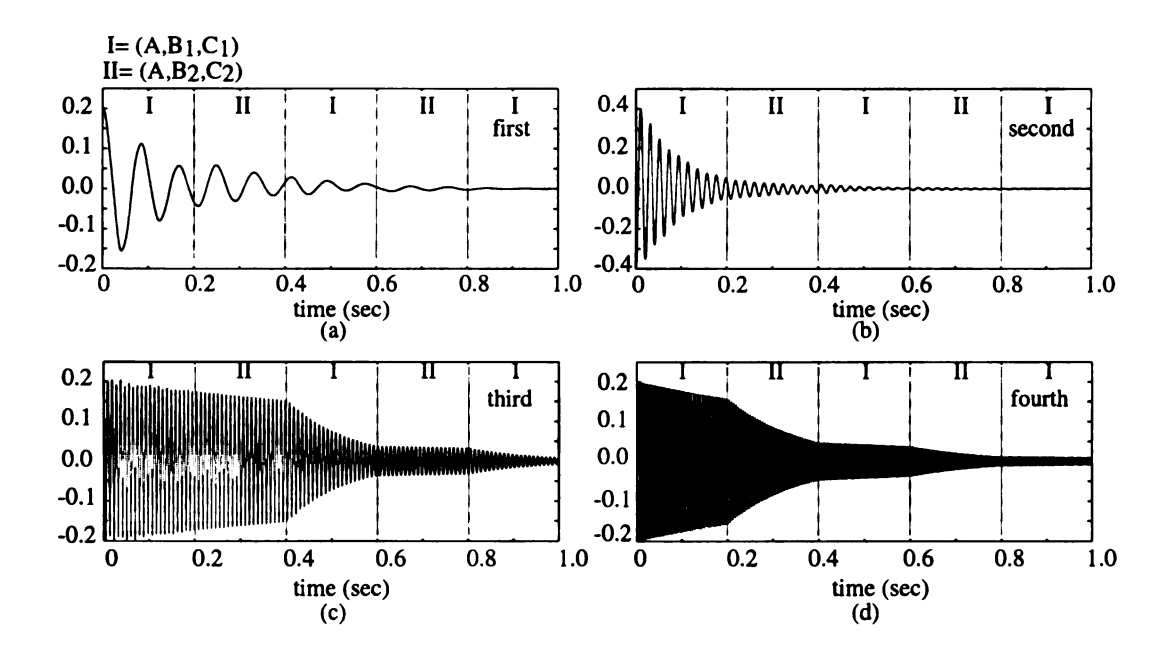


Figure 3.4. Amplitude of vibration of the (a) first, (b) second, (c) third, and (d) fourth modes of the beam with observer-based control design

The time duration of simulation is 1.0 sec and switching occurred at 0.2, 0.4, 0.6 and 0.8 secs, starting with the system with the description  $(A, B_1, C_1)$ . These results indicate that the first and second modes of vibration, which are controllable and observable for both system descriptions in Equations (3.17), are attenuated rapidly and continuously. The fourth mode is observable for the system description  $(A, B_1, C_1)$  and controllable for the description  $(A, B_2, C_2)$ . Therefore it is rapidly attenuated during all time intervals where the system description is  $(A, B_2, C_2)$ , namely, second interval, fourth interval, and so on. The attenuation during the first, third, and fifth intervals are due to structural damping. The third mode is observable for the

system description  $(A, B_2, C_2)$  and controllable for the description  $(A, B_1, C_1)$ . This mode is rapidly attenuated during all time intervals where the system description is  $(A, B_1, C_1)$ , except the first interval since observability is required prior to controllability for the purpose of control.

The results in this section indicate that we are able to sense and control all four modes of the beam using two piezoelectric elements only. With dedicated and collocated sensors and actuators, we would have used two piezoelectric elements as actuators and an additional two elements as sensors. This would require two power amplifiers for the two actuators and two analog-to-digital conversion channels in our data acquisition hardware for the two sensors. Clearly, our approach has halved the number of piezoelectric elements, the number of power amplifiers, and the number of data acquisition channels, required for sensing and control.

### 3.6 Sub-optimal switching schedule

By substituting the feedback laws of Equation (3.19) into Equation (3.17), we get the two closed-loop systems

$$\dot{X} = A_{c1}X, \qquad \dot{X} = A_{c2}X \tag{3.21}$$

where  $X \triangleq (x^T, \ \widehat{x}^T)^T$  and

$$A_{ci} = \begin{bmatrix} A & -B_i K_i \\ L_i C_i & A - B_i K_i - L_i C_i \end{bmatrix}$$
 (3.22)

Given a total time duration of  $t_f$  secs and m switchings, our goal is to find the switching times  $t_i$ ,  $i=1,2,\cdots m$ , that satisfy  $0 \le t_1 \le t_2 \cdots \le t_m \le t_f$  and minimizes the cost function

$$J = \int_0^{t_f} X^T Q X \, dt \tag{3.23}$$

where Q is a constant positive definite matrix. Both  $A_{c1}, A_{c2} \in R^{2(p+q+r)}$  have 2p+q+r eigenvalues with strictly negative real parts by virtue of pole placement. The q+r remaining eigenvalues correspond to the uncontrollable and unobservable states and have zero real parts or small negative real parts depending on the level of structural damping. Consequently, we can solve the Lyapunov equations

$$A_{c1}^T P_1 + P_1 A_{c1} = -Q, \qquad A_{c2}^T P_2 + P_2 A_{c2} = -Q$$
 (3.24)

to obtain unique solutions for  $P_1$  and  $P_2$ . Assuming the closed-loop system matrix to be  $A_{c1}$  at the initial time, the cost function in Equation (3.23) can be written as

$$J = -\int_{0}^{t_{1}} \frac{\partial}{\partial t} \left( X^{T} P_{1} X \right) - \int_{t_{1}}^{t_{2}} \frac{\partial}{\partial t} \left( X^{T} P_{2} X \right) - \int_{t_{2}}^{t_{3}} \frac{\partial}{\partial t} \left( X^{T} P_{1} X \right) - \int_{t_{3}}^{t_{4}} \frac{\partial}{\partial t} \left( X^{T} P_{2} X \right) - \cdots$$

$$(3.25)$$

and then simplified to the form

$$J = X(0)^{T} P_{1} X(0) - X(t_{f})^{T} P_{*} X(t_{f}) + X(t_{1})^{T} (P_{2} - P_{1}) X(t_{1})$$

$$- X(t_{2})^{T} (P_{2} - P_{1}) X(t_{2}) + \cdots + X(t_{m})^{T} (P_{2} - P_{1}) X(t_{m})$$
(3.26)

where  $P_*$  equals  $P_1$  for even number of switchings and  $P_2$  for odd number of switchings, and the sign of the last term in Equation (3.26) is positive for odd number of switchings and negative for even number of switchings. Since the states and their estimates at  $t = t_1, t_2, \cdots$  can be defined iteratively as follows

$$X(t_1) = \exp[A_{c1}t_1]X(t_0)$$
 (3.27a)

$$X(t_2) = \exp[A_{c2}(t_2 - t_1)]X(t_1)$$
 (3.27b)

34

the cost function in Equation (3.23) can be expressed as

$$J = X^{T}(t_0)HX(t_0) (3.28)$$

where H is a positive definite matrix that is a function of  $t_1, t_2, \dots, t_m$ . With the objective of minimizing J, we rewrite Equation (3.27) as

$$J = \operatorname{trace}[J] \tag{3.29a}$$

$$= \operatorname{trace} \left[ X^{T}(t_0) H X(t_0) \right] \tag{3.29b}$$

$$= \operatorname{trace} \left[ HX^{T}(t_{0})X(t_{0}) \right]$$
 (3.29c)

$$= \operatorname{trace} \left[ HX^{T}(t_0)X(t_0) \right]$$
 (3.29d)

$$\leq \operatorname{trace}[H]||X(t_0)||^2 \tag{3.29e}$$

Since the initial state,  $X(t_0)$ , is unknown, we propose to minimize J by minimizing trace [H]. This approach, which has been proposed earlier ([55], [56], for example) results in upper-bound minimization since

$$X^{T}(t_0)HX(t_0) \le \lambda_{max}(H) ||X(t_0)||^2 \le \text{trace}[H] ||X(t_0)||^2$$
 (3.30)

We minimize the upper bound by solving

$$t_1, t_2, \cdots, t_m = \arg \left\{ \min(\operatorname{trace}[H]) \right\}$$
 (3.31)

subject to  $0 < t_1 < t_2 < \cdots < t_m \le t_f$ . We choose to minimize the upper bound rather than the maximum eigenvalue of H since trace [H] can be easily expressed as a function of the switching times,  $t_1, t_2, \cdots, t_m$ , unlike  $\lambda_{max}(H)$  which cannot be expressed in terms of the switching times. However, since we minimize the upper bound of  $X^T(t_0)HX(t_0)$ , our solution is sub-optimal and not optimal. The sub-

optimal switching instants are also solved in an open-loop fashion and is not based on state feedback. The simulation results for sub-optimal switching, based on the identity Q matrix and the initial conditions in Equation (3.20), are shown in Figure(3.5). The time duration of simulation is 1.0 sec and the number of switchings is set to four. This allows us to compare the results with the simulation results in Figure(3.4). The sub-optimal switching instants were obtained as  $t_1=0.01,\,t_2=0.02,\,t_3=0.1,$  and  $t_4=0.37.$  A close look at the results obviates that the transient response is better for the case with sub-optimal switching than the case with switching at regular intervals.

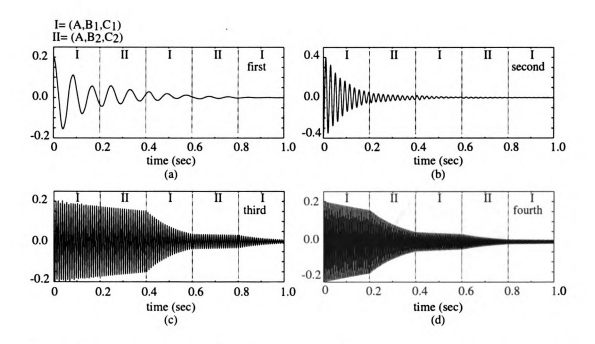


Figure 3.5. Amplitude of vibration of the (a) first, (b) second, (c) third, and (d) fourth modes of the beam with sub-optimal switching

### 3.7 Experimental verification

#### 3.7.1 Apparatus

In order to demonstrate feasibility of switching piezoelectric transducers between actuator and sensor modalities and obviate the merit of introducing under-actuation and under-sensing, we performed experiments with the flexible cantilever beam shown in Figure (3.6). Although we used a simply supported beam in our simulations in Sections 3.5 and 3.6, we used a cantilever beam in our experiments since the experimental setup is simpler and the modal frequencies are lower for the cantilever beam. With lower modal frequencies, the task of real-time data acquisition and control becomes easier.

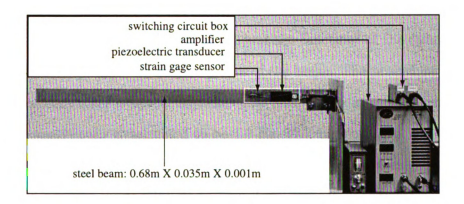


Figure 3.6. Experimental test-rig

In our experiments, we used a single piezoelectric element\* to sense and control the first two modes of the beam. Both the modes are controllable but unobservable when the element is used as an actuator, and observable but uncontrollable when it is used as a sensor. Our experimental results will establish that we are able to obtain

<sup>\*</sup>manufactured by Mide Technology Corporation [57]

complete controllability and observability by continuously switching the modality of the single piezoelectric element. This reduces the number of piezoelectric elements required by 50% since two elements, one dedicated as an actuator and the other dedicated as a sensor, would be typically used for sensing and controlling the two modes. With the dedicated actuator and sensor pair, we would have required one power amplifier and one data acquisition channel. Our experiments also required one amplifier and one data acquisition channel but both the amplifier and the data channel were used only 50% of the time. In a setup with two piezoelectric elements, similar to the one used in simulations, a single amplifier and a single data acquisition channel would suffice since they would be time-shared between the two piezoelectric elements. In such a setup, under-actuation and under-sensing would contribute to greater cost and weight savings. In our experiments, the strain gage sensor † was only used for experimental determination of the transfer function<sup>‡</sup> of the dynamic system representative of the first two flexible modes of the beam. The procedure for transfer function determination is described next. The first three natural frequencies of the beam were analytically determined to be 1.8 Hz, 11.3 Hz, and 31.6 Hz, respectively. To model the first two modes of the beam only, we excited the piezoelectric element sinusoidally over the range 0-20 Hz and used the voltage output of the strain gage sensor,  $Y_{sg}(s)$ , to compute the gain and phase lag of the system. Using Matlab, the transfer function that best fit the gain and phase plots was determined to be

$$G_1(s) = \frac{Y_{sg}(s)}{U(s)} = 2.475 \frac{s^2 + 0.7775s + 748.5}{(s^2 + 0.452s + 127.7)(s^2 + 2.6s + 4225)}$$
(3.32)

From the structure of the transfer function in Equation (3.32), it is clear that the system is completely controllable and observable with the piezoelectric element as

<sup>†</sup>manufactured by PCB Piezotronics, Inc. [58]

<sup>&</sup>lt;sup>‡</sup>between voltage input to the piezoelectric element (used as actuator) and voltage output of the same element (used as sensor)

actuator and the strain gage sensor. A complete modal state space representation of the system was therefore obtained as follows

$$A = \begin{bmatrix} 0.0 & 0.0 & 1.0 & 0.0 \\ 0.0 & 0.0 & 0.0 & 1.0 \\ -127.69 & 0 & -0.45 & 0 \\ 0.0 & -4225.0 & 0.0 & -2.60 \end{bmatrix} B = \begin{bmatrix} 0.0 \\ 0.0 \\ 2.5 \\ 10 \end{bmatrix} C = \begin{bmatrix} 0.15 \\ 0.21 \\ 0.0 \\ 0.0 \end{bmatrix}$$
(3.33)

which obviously satisfies  $G_1(s) = C(sI - A)^{-1}B$ . Our desired transfer function, between voltage input to the piezoelectric element (used as actuator) and voltage output of the same element (assuming it is simultaneously used as sensor),  $Y_{pzt}(s)$ , was obtained using the relation

$$G(s) = \frac{Y_{pzt}(s)}{U(s)} = \overline{C}(sI - A)^{-1}B, \qquad \overline{C} \triangleq [0.15\alpha_1, \ 0.21\alpha_2, \ 0.0, \ 0.0]$$
 (3.34)

where  $\alpha_1$  and  $\alpha_2$  denote the ratios of the output of the piezoelectric sensor and the strain gage, corresponding to the first and second modes of vibration, respectively.

In continuation first, we discuss the combination of analytical and experimental methods used in determining  $\alpha_1$  and  $\alpha_2$  in Equation (3.34). The voltage output of the piezoelectric sensor,  $V_{pzt}$ , and the strain gage sensor,  $V_{sg}$ , can be expressed as

$$V_{pzt} = K_{pzt} \frac{\partial^2 y(x_{pzt}, t)}{\partial t^2}, \qquad V_{sg} = K_{sg} \frac{\partial^2 y(x_{sg}, t)}{\partial t^2}$$
 (3.35)

where  $K_{pzt}$  and  $K_{sg}$  are constants that are characteristic of the piezoelectric sensor and strain gage sensor, respectively, and  $x_{pzt}$  and  $x_{sg}$  are the locations of the two sensors, respectively. In Equation (3.34),  $\alpha_1$  and  $\alpha_2$  are equal to the ratio  $(V_{pzt}/V_{sg})$  when the beam is oscillating purely in the first and second modes, respectively. By deflecting the tip of the beam and releasing it, the beam was made to oscillate purely

in the first mode. During such motion,  $V_{pzt}$  and  $V_{sg}$  were measured and their ratio computed. This ratio, which was found to be approximately constant, is equal to  $\alpha_1$ . With the knowledge of  $\alpha_1$  and by numerically evaluating  $\partial^2 y(x_{pzt},t)/\partial t^2$  and  $\partial^2 y(x_{sg},t)/\partial t^2$  for the first mode, we were able to obtain the ratio  $K_{pzt}/K_{sg}$ . We next evaluated  $\partial^2 y(x_{pzt},t)/\partial t^2$  and  $\partial^2 y(x_{sg},t)/\partial t^2$  for the second mode and with the knowledge of  $K_{pzt}/K_{sg}$ , we computed  $\alpha_2$ .

In our case, these ratios were found to be  $\alpha_1 = 3.33$  and  $\alpha_2 = 33.33$ . Therefore, G(s) was described by the A and B matrices in Equation (3.33) and the new output description matrix  $\overline{C} = (0.5, 7.0, 0.0, 0.0)^T$ .

We complete this section with a discussion of the hardware used for data acquisition, control, and switching. We programmed our control law and switching algorithm in Matlab/Simulink $^{TM}$  environment and downloaded it to our dSPACE DSP board, shown in Figure(3.7). The DSP Board reads the measured signals when the piezoelectric transducer is in the sensor mode and estimates the states of the flexible beam. When the transducer is switched to actuator mode, the estimated states are used to compute the control input required for suppressing the vibration in the beam. The computed control signal is sent to the power amplifier which provides the voltage required for actuating the piezoelectric transducer. A trigger signal is used to switch the piezoelectric transducer between actuator and sensor modes. For a very short time interval, prior to triggering the transducer from actuator mode to sensor mode, the voltage commanded to the transducer is set to zero. This enables us to switch to the sensor mode with zero initial conditions.

### **3.7.2** Results

The piezoelectric transducer in our experimental hardware guarantees observability of several modes of the beam, including the first two, and hence the voltage output of the transducer,  $y_{pzt}(t)$ , is a good measure of vibration of the beam. Our

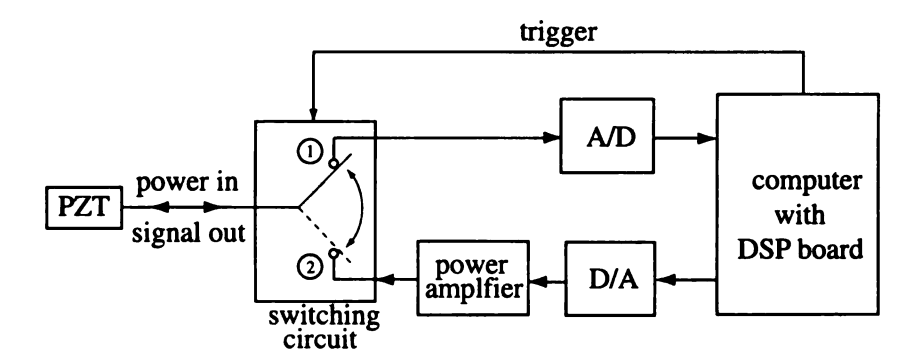


Figure 3.7. Schematic of switching between actuator and sensor modalities

experimental results are shown in Figure (3.8). In each of these experiments, the beam was set into vibration by displacing the beam-tip 5 cms (corresponds to maximum sensor output of 10 volt in dynamic mode) and releasing it at the initial time. The initial condition (in modal coordinates) was therefore a nonzero value for the first state  $\eta_1$  in Equation (2.28) and zero values for the other three states,  $\eta_2$ ,  $\dot{\eta}_1$ , and  $\dot{\eta}_2$ .

The first experiment, shown in Figure (3.8)(a), pertains to free vibration of the beam. In the absence of control, the beam vibration is attenuated slowly by the structural damping. The time required for the amplitude of vibration to decay by a factor of 25 is approximately 50 secs.

The second experiment, shown in Figure (3.8)(b), pertains to vibration suppression using the single piezoelectric transducer, switching on a fixed-time schedule. In this experiment, the transducer was switched between actuator and sensor modes with a time period of 1 sec. Within the 1 sec duration, the transducer was used as a sensor for 300 msecs and as an actuator for 700 msecs. Figure (3.8)(b) shows the transducer output only during the time intervals it was used as a sensor. The effectiveness of the switching observer-based controller is clear from the time required for vibration attenuation, which is only 12 secs as compared to 50 secs in Figure (3.8)(a).

A closer look at A closer look at Figure (3.8)(b) indicates that the switching observer-based controller excites the higher modes of the beam. Though these modes

die out because of structural damping, they can have detrimental effects. The excitation of the higher modes is attributed to the discontinuous controls profile generated by the fixed-time switching schedule of our algorithm. This is further explained with the help of Figure(3.9)(b). To avoid discontinuous inputs, we adopted a variable-time switching schedule where the piezoelectric transducer is switched (both from sensor mode to actuator mode and from actuator mode to sensor mode) at the first instance when the control input is zero, beyond the time proposed by the fixed-time switching schedule. The variable-time switching schedule is explained with the help of Figure(3.9)(c). The results obtained with variable-time switching are shown in Figure(3.8)(c) and here the switching times, t = 0.61, t = 1.08, t = 1.51, and t = 2.21, for example, are the first instants of time when u = 0 after t = 0.30, t = 1.00, t = 1.30, and t = 2.00, respectively. It can be seen from the Figure(3.8)(c) that the higher modes are not excited.

The experimental results in Figure (3.8)(d) pertains to a sub-optimal switching schedule with m=10 switchings and  $t_f=5$  secs. We chose m=10 and  $t_f=5$  to compare the results with those obtained from the fixed-time switching schedule (Figure (3.8)(b)), which also switches 10 times during 5 secs. The optimal switching instants were obtained apriori using the Nelder-Mead simplex search in Matlab as

$$t_1, t_2, \cdots, t_{10} = 0.254, 0.924, 1.459, 1.911, 2.267, 2.966, 3.472, 3.938, 4.267, 4.745$$

$$(3.36)$$

A comparison of the amplitudes of vibration in Figure (3.8)(b), Figure (3.8)(c), and Figure (3.8)(d) indicate that the sub-optimal switching schedule is more effective in attenuating vibration that the fixed-time and the variable-time switching schedules.

We conclude this section with a discussion on the variable-time switching schedule which was adopted in our experiments to avoid excitation of higher unmodeled modes of the beam. Consider an observer-based feedback control law,  $u = K\hat{x}$ , which has

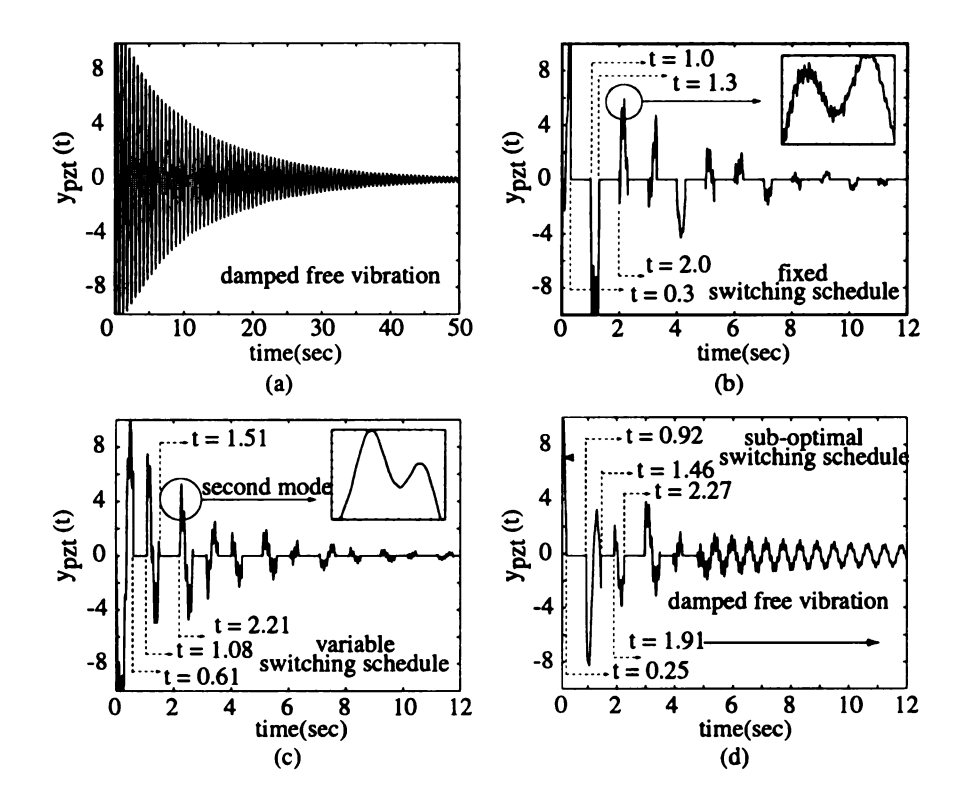


Figure 3.8. Experimental results: Plot of  $y_{pzt}$  with time for (a) uncontrolled system, and controlled system with (b) fixed switching schedule, (c) variable switching schedule, and (d) sub-optimal switching schedule.

the profile shown in Figure (3.9)(a). For our experiments, where a single piezoelectric transducer was used,  $\hat{x}$  was obtained using a closed-loop observer when the transducer was in the sensor mode, and obtained using an open-loop observer when the transducer was in the actuator mode. Now consider the fixed-time switching schedule used in our experiments, where the piezoelectric transducer was alternately used as a sensor for 300 msecs, and as an actuator for 700 msecs. For this switching schedule, our control input would have the profile shown in Figure (3.9)(b). The control input would be discontinuous due to the fixed-time nature of the switching and this would excite higher unmodeled modes of the beam. This has been seen in our experimental results in Figure (3.8)(b). To alleviate this problem, which is caused by discontinuity in the input, we delayed switching (both from actuator mode to sensor mode and sensor mode to actuator mode) till the first instance of time when the control in-

put is zero. Such a switching schedule results in the control input profile shown in Figure (3.9)(c). Although the control input is non-smooth, it is continuous and therefore does not excite the higher-order unmodeled dynamics of the beam. This can be verified from our experimental results in Figure (3.8)(c).

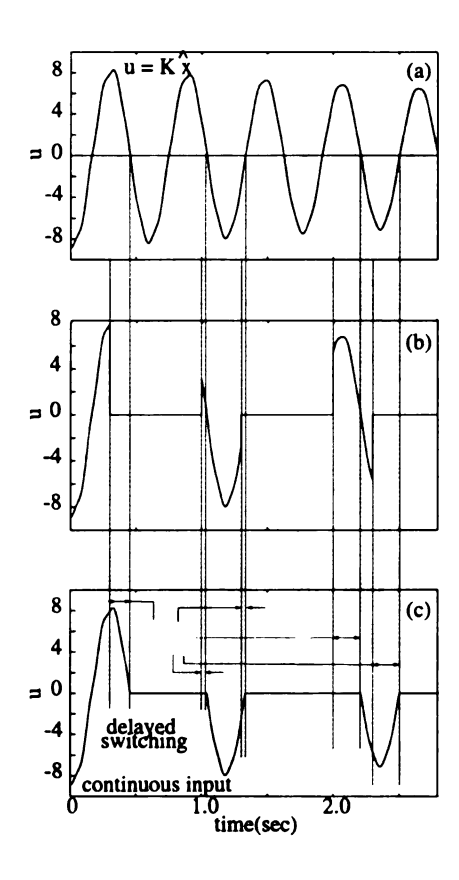


Figure 3.9. (a) An observer-based controller (b) a discontinuous and (c) a continuous controller obtained from using a fixed-time and variable-time switching schedule..

## CHAPTER 4

# Vibration Control of a Flexible Beam using an End Force

### 4.1 Background

In this chapter we propose a novel approach in vibration suppression of a flexible beam. In a deviation from the traditional approach, we propose to estimate the significant modes of the system using piezoelectric sensors but control them using an end-force instead of piezoelectric actuators. Our goal is to introduce a control strategy to switch the end-force on and off to suppress vibrations of the beam. The equation governing the lateral vibration of the beam is nonlinear with respect to the end force. This was shown in Chapter 2. Furthermore, the end force can only be applied unidirectionally. These two facts necessitate the use of nonlinear control tools for design of a feedback law. In this work we use Lyapunov stability theory along with passivity-based methods to design a stabilizing control for the closed loop system.

# 4.2 Mathematical model of cantilever beam with end-force

Consider the cantilever beam of length L and uniform cross-sectional area A, shown in Figure (4.1). Let P be the force acting at the free end of the beam such that its line of action always passes through the fixed end of the beam. It was shown in Chapter 2

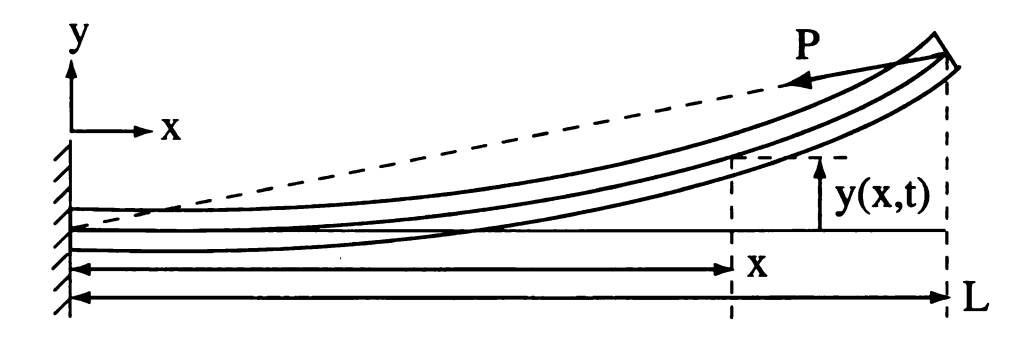


Figure 4.1. A flexible cantilever beam with an end force

that under the assumption of Euler-Bernoulli beam theory and small deflections the equation of motion of the beam can be written as follows

$$EIy'''' + Py'' + \rho A\ddot{y} = 0 \tag{4.1}$$

where E, I, and  $\rho$  are the Young's modulus of elasticity, area moment of inertia, and density of the beam, respectively, and y' and  $\dot{y}$  denote the partial derivatives of y(x,t) with respect to x and t, respectively. Equation (4.1), is identical to the equation of a beam with a follower end force [21] and a beam with an axial end force whose line is action remains parallel to the undeformed axis of the beam. The boundary conditions of the beam in Figure (4.1) are however different from beams with follower and axial end forces. The geometric boundary conditions, which are related to zero deflection

and zero slope at the fixed end, are

$$y(0,t) = 0,$$
  $y'(0,t) = 0$  (4.2)

The natural boundary conditions corresponding to zero moment and nonzero shear force at the free end are given by the relations

$$y''(L,t) = 0,$$
  $EIy'''(L,t) + P\left\{y'(L,t) - \frac{1}{L}y(L,t)\right\} = 0$  (4.3)

For small deflections, the end force in Figure (4.1) can be decomposed into a force of magnitude P along the negative x axis and a force of magnitude Py(L,t)/L along the negative y axis. The component along the x axis is constant and is therefore conservative. The component along the y axis is also conservative since it is proportional to the displacement of the point of application, similar to a spring force. Our end force is therefore conservative despite is close resemblance to a follower force, which is nonconservative in nature [21]. This distinction is important since the Euler method of determining elastic stability is applicable for conservative external forces only [21]. Now consider the elastic stability problem for the beam with end force, as shown in Figure (4.1). For a small static deformation, the differential equation of the beam can be obtained by substituting y(x,t) = Y(x),

$$EIY'''' + PY'' = 0, \qquad Y' \triangleq \frac{dY}{dx} \tag{4.4}$$

The solution to this differential equation has the form

$$Y(x) = \beta_1 + \beta_2 x + \beta_3 \sin(\alpha x) + \beta_3 \cos(\alpha x), \quad \alpha \triangleq \sqrt{\frac{P}{EI}}$$
 (4.5)

where  $\beta_i$ , i = 1, 2, 3, 4, are constants that can be determined from the boundary conditions in Equation (4.2, 4.3), namely,

$$Y(0) = 0, \quad Y'(0) = 0, \quad Y''(L) = 0, \quad Y'''(L) + \alpha^2 \left\{ Y'(L) - \frac{Y(L)}{L} \right\} = 0 \tag{4.6}$$

Equation (4.6) can be explicitly written in terms of the constants  $\beta_i$ , i = 1, 2, 3, 4, as follows

$$\begin{bmatrix} 1 & 0 & 0 & 1 \\ 0 & 1 & \alpha & 0 \\ 0 & 0 & \sin(\alpha L) & \cos(\alpha L) \\ 1 & 0 & \sin(\alpha L) & \cos(\alpha L) \end{bmatrix} \begin{bmatrix} \beta_1 \\ \beta_2 \\ \beta_3 \\ \beta_4 \end{bmatrix} = \begin{bmatrix} 0 \\ 0 \\ 0 \\ 0 \end{bmatrix}$$

$$(4.7)$$

and the non-trivial solutions can be obtained by equating the determinant of the matrix in Equation (4.7) equal to zero. The determinant of the matrix is  $\sin(\alpha L)$  and by equating it to zero, we get

$$\alpha_n = \frac{n\pi}{L}, \quad n = \pm 1, \pm 2, \dots \implies P_{cr} = n^2 \pi^2 \frac{EI}{L^2}$$
 (4.8)

The above result establishes that the beam in Figure (4.1) first buckles when  $P = \pi^2 EI/L^2$ . This load is four times larger than the buckling load for a cantilever beam with an axial end force [21], [60]. This implies that we can use a relatively large end force on our beam for vibration control without creating instability. Before we complete this section, we would like to point out that the buckling nature of the end force in Figure (4.1) is deduced from the fact that the matrix in Equation (4.7), looses rank and has an eigenvalue at zero when P assumes a critical value. For a follower type end force, which is non-conservative in nature, the corresponding matrix is always nonsingular. As the magnitude of the follower force is increased, two distinct eigenvalues of the matrix approach each other, assume the same value at the critical load, and then become complex resulting in flutter instability [21].

### 4.3 Rayleigh-Ritz approximation

In order to obtain an approximate solution to Equation (4.1) subject to the boundary conditions in Equation (4.2, 4.3), we multiply Equation (4.1) with a weight function w(x), and integrate it over the length of the beam

$$\int_0^L EI w(x) y''''(x,t) dx + \int_0^L P w(x) y''(x,t) dx + \int_0^L \rho A w(x) \ddot{y}(x,t) dx = 0 \quad (4.9)$$

We simply assume that w(x) is continuous, twice differentiable, and satisfies the two geometric boundary conditions in Equation (4.2), namely

$$w(0) = 0, w'(0) = 0 (4.10)$$

In order to distribute the derivatives equally between y(x,t) and w(x), we integrate the first integral in Equation (4.9) twice by parts, and the second integral once by parts, to get

$$\left(EIw\,y''' - EIw'\,y'' + Pwy'\right)\Big|_0^L + \int_0^L \left(EI\,w''\,y'' - P\,w'\,y' + \rho A\,w\,\ddot{y}\right)dx = 0 \quad (4.11)$$

Equation (4.11) is called the weak form [61] of Equation (4.1). Using the natural boundary conditions of y in Equation (4.3) and the geometric boundary conditions of w in Equation (4.10), we get

$$P \frac{w(L) y(L,t)}{L} + \int_0^L \left( EI w'' y'' - P w' y' + \rho A w \ddot{y} \right) dx = 0$$
 (4.12)

We now use Rayleigh-Ritz approximation [61] to express y(x,t) as a linear combination of N suitable functions that satisfy the geometric boundary conditions in Equation (4.2). Specifically, we use the first N normalized mode shapes of the clamped-free cantilever beam, as follows

$$y_N(x,t) = \sum_{i=1}^{N} a_i(t) \,\phi_i(x) \tag{4.13}$$

In the above equation,  $\phi_i(x)$ ,  $i=1,2,\cdots,N$ , are the assumed modes, N is the number of desired modes, and  $a_i(t)$ ,  $i=1,2,\cdots,N$ , are the corresponding modal displacements. Now, by choosing  $y(x,t)\approx y_N(x,t)$  and  $w(x)=\phi_j(x)$ ,  $j=1,2,\cdots,N$ , consistent with Equation (4.8), we get N differential equations from Equation (4.12), as follows

$$EI \sum_{i=1}^{N} \left( \int_{0}^{L} \phi_{i}^{"} \phi_{j}^{"} dx \right) a_{i} - P \sum_{i=1}^{N} \left( \int_{0}^{L} \phi_{i}^{'} \phi_{j}^{'} dx - \frac{\phi_{i}(L) \phi_{j}(L)}{L} \right) a_{i} + (4.14)$$

$$\rho A \sum_{i=1}^{N} \left( \int_{0}^{L} \phi_{i} \phi_{j} dx \right) \ddot{a}_{i} = 0, \qquad j = 1, 2, \dots, N$$

Using the orthogonality property of the assumed mode shapes, the above N equations can be written as follows

$$\ddot{a} + (K - PC) a = 0 (4.15)$$

where  $a \triangleq (a_1, a_2, \dots, a_N)^T$ ,  $K \in \mathbb{R}^{N \times N}$  is a diagonal positive definite matrix with elements  $K_{ii}$ ,  $C \in \mathbb{R}^{N \times N}$  is a positive definite symmetric matrix [62] with elements  $C_{ij}$ , and P is assumed to be positive in the direction shown in Figure (1). The elements  $K_{ii}$  and  $C_{ij}$  have the following expressions

$$K_{ii} \triangleq \frac{EI}{\rho A} \int_0^L \left[ \phi_i''(x) \right]^2 dx, \quad C_{ij} \triangleq \frac{1}{\rho A} \int_0^L \left[ \left( \phi_i'(x) \, \phi_j'(x) \, dx - \frac{\phi_i(L) \, \phi_j(L)}{L} \right) \right] \tag{4.16}$$

Earlier, we claimed in Section 4.2 that the end force in Figure (4.1) is conservative in nature. This can now be claimed [63] from the symmetric nature of the matrix (K - PC) in Equation (4.15).

When P = 0, the eigenvalues of (K - PC) are the same as the eigenvalues of K, which are all positive. As P is increased, all the eigenvalues start moving towards the origin. The end force P assumes a critical value, given by Equation (4.8), every time one of the eigenvalues reaches the origin before crossing the imaginary axis and becoming negative. This can be claimed from the physics of the buckling problem and has also been verified using numerical simulations.

In the derivation of Equation (4.15), structural damping was assumed absent. If structural damping is present, we can use

$$\ddot{a} + D\dot{a} + (K - PC)a = 0 \tag{4.17}$$

where where  $D \in \mathbb{R}^{N \times N}$  is a diagonal positive definite matrix of modal damping.

# 4.4 Preliminary feedback control design

In order to design a feedback controller for vibration suppression, we first rewrite Equation (4.17) in state space form

$$\dot{x}_1 = x_2 \tag{4.18a}$$

$$\dot{x}_2 = -Kx_1 - Dx_2 + Cx_1 u \tag{4.18b}$$

where  $x_1 \triangleq a \in \mathbb{R}^N$  and  $x_2 \triangleq \dot{a} \in \mathbb{R}^N$  are the state variables, and  $u \triangleq P \in \mathbb{R}$  is the control input. The task of vibration suppression in the beam can be posed as a problem of design of the control input u that satisfies the constraint

$$0 \le u < \pi^2 EI/L^2 \tag{4.19}$$

and guarantees asymptotic stability of the equilibrium point  $(x_1, x_2) = (0, 0)$ . The constraints on the input are necessary since  $u \ge \pi^2 EI/L^2$  results in buckling instability and u < 0 cannot be physically applied using a cable. We present our preliminary control design next with the help of the following Theorem.

**Theorem 1:** (Asymptotic Stability) The origin of the system described by Equation (4.18) is rendered globally asymptotically stable by the following choice of input u(t),

$$u(t) = \begin{cases} P_0 & \text{if } x_2^T C x_1 < 0\\ 0 & \text{if } x_2^T C x_1 \ge 0, \end{cases} \qquad 0 < P_0 < \pi^2 E I / L^2 \qquad (4.20)$$

independent of the amount of structural damping present in the system.

**Proof:** Consider the Lyapunov function candidate

$$V_1(x_1, x_2) = \frac{1}{2} \left( x_1^T K x_1 + x_2^T x_2 \right) \tag{4.21}$$

It is positive everywhere other than the origin where it is equal to zero. The derivative of the Lyapunov function candidate is

$$\dot{V}_1 = x_1^T K x_2 + x_2^T (-K x_1 - D x_2 + C x_1 u) 
= -x_2^T D x_2 + (x_2^T C x_1) u$$
(4.22)

For the choice of control input in Equation (4.20), it can be easily shown that  $\dot{V}_1 \leq 0$  and  $\dot{V}_1 = 0$  iff  $x_2 = 0$ . Using LaSalle's Theorem [59] we can therefore claim that the origin is asymptotically stable. Since  $V_1$  is radially unbounded, the origin is globally asymptotically stable.  $\diamond \diamond \diamond$ 

Remark: The control law in Equation (4.20) essentially implies that the bucklingtype end force should be turned "on" whenever it can do negative work or remove energy from the system, and kept "off" at all other times.

We now investigate the efficacy of the control design in Equation (4.20) using simulation. We assumed the material and geometric properties of the beam to be:

Material Alluminum

Young's modulus 70 GPa

Mass density  $2730 \text{ kg/m}^3$ 

Dimensions  $1.00 \times 0.05 \times 0.003 \text{ m}$ 

For a two-mode approximation of beam dynamics, the K, C, and D matrices of our mathematical model in Equation (4.18) were computed as

$$K = \begin{pmatrix} 97.38 & 0 \\ 0.0 & 3824.39 \end{pmatrix}, C = \begin{pmatrix} 1 & -5.28 \\ -5.28 & 44.41 \end{pmatrix}, D = \begin{pmatrix} 0.098 & 0 \\ 0.0 & 0.618 \end{pmatrix}$$
(4.23)

The square root of the diagonal entries of the K matrix are the natural frequencies of the beam and are equal to 9.87 rad/s and 61.84 rad/s, respectively. The critical buckling load of the beam was computed to be approximately 50N using Equation (4.8). It can also be obtained by computing the minimum eigenvalue of  $-C^{-1}K$ . For the sake of simplicity, we assumed proportional damping (no modal coupling). The diagonal entries of the D matrix in Equation (4.23) correspond to  $\zeta = 0.005$ . We chose  $P_0$  in Equation (4.20) less than the critical buckling load, and equal to 35 N. The simulation results are shown in Figure (4.2) for the following initial conditions in SI units

$$x_1(0) = \begin{bmatrix} a_1(0) \\ a_2(0) \end{bmatrix} = \begin{bmatrix} 0.1 \\ 0.0 \end{bmatrix}, \qquad x_2(0) = \begin{bmatrix} \dot{a}_1(0) \\ \dot{a}_2(0) \end{bmatrix} = \begin{bmatrix} 0.0 \\ 0.0 \end{bmatrix}$$
(4.24)

In Figure (4.2)(a) we plot the amplitude of the first mode in the absence of control. It

decays to zero very slowly due to low structural damping. The amplitude of the second mode, in the absence of control, is not shown in Figure (4.2) since it is identically zero. This is true since the modal dynamics in Equation (4.18) are decoupled (K) and (C) matrices are diagonal) in the absence of control. The plots in Figure (4.2)(b) and (C) show the modal amplitudes as a function of time for the control action in Equation (4.20). The control action itself is plotted in Figure (4.2)(d). A number of observations can be made from the simulation results in Figure (4.2)(b), (c), and (d):

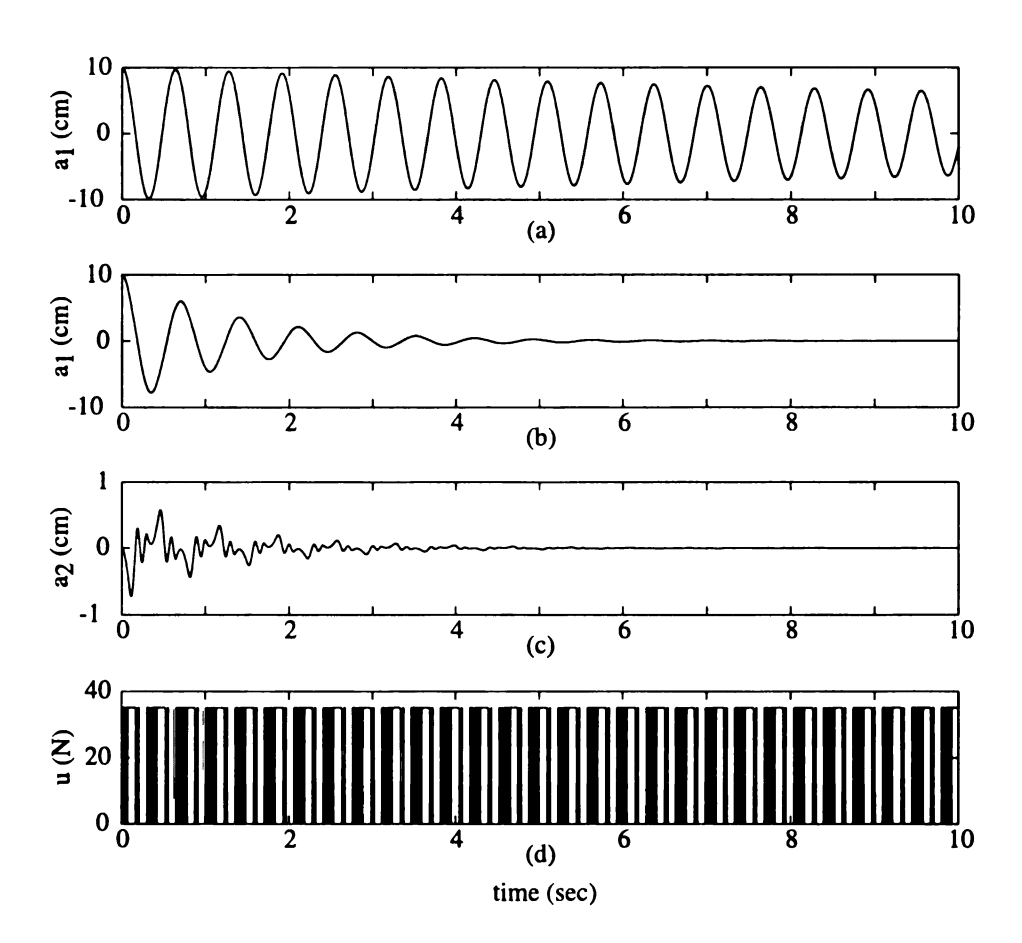


Figure 4.2. Simulation of decay in modal amplitude  $a_1$  due to structural damping, (b), (c) decay in modal amplitudes  $a_1$  and  $a_2$  due to control in the presence of structural damping, and (d) plot of the control action.

- 1. The modal amplitudes,  $a_1$  and  $a_2$ , rapidly decay to zero, as expected, but the control input keeps on switching. This can be attributed to small numerical errors causing frequent change in sign of the term  $x_2^T C x_1$  and the particular nature of our control law in Equation (4.20). This problem can be easily rectified during actual implementation.
- 2. Due to the particular structure of matrix C, the modal dynamics in Equation (4.18) is coupled. This is evident from the vibration of the second mode despite zero initial conditions.
- 3. The main advantage of the control law in Equation (4.20) is that it can be implemented using state feedback for as many modes as we desire to model. However, it has one major drawback. The term  $x_2^T C x_1$  will have many frequency components (the highest frequency component will be twice the highest modal frequency) and it will change sign rapidly. This may easily exceed the bandwidth of the actuator used to switch the end force. If the actuator does not have the requisite bandwidth, the closed-loop system will most likely become unstable since incorrect timing of switching will tantamount to adding energy to the system.

One way to circumvent the requirement of high actuator bandwidth is to discard the high frequency components using a low-pass filter in the control loop without adversely affecting the stability of the system. This is achieved using our control design presented in the next section.

### 4.5 Modified control design

Our dynamical system described by Equation (4.18) can be represented by the inputoutput mapping shown in Figure (4.3)

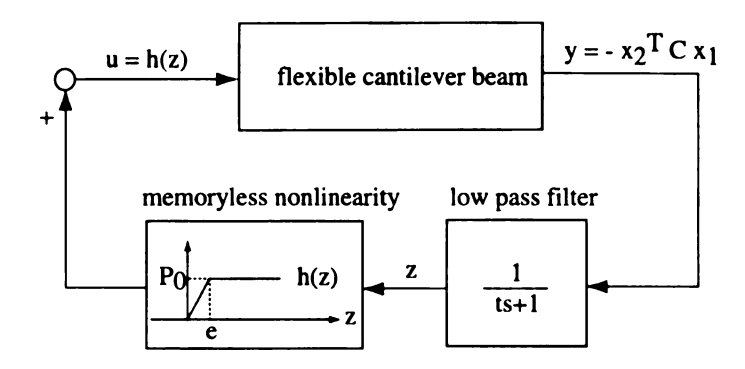


Figure 4.3. Control design based on output filtering.

where, u represents our buckling-type end force and y represents the output, defined as follows

$$y = -x_2^T C x_1 (4.25)$$

Now consider the feedback connection in Figure (4.3) where the input to our dynamical system is obtained by feeding the output of our system through a low-pass filter (of time constant  $\tau$  and unity dc gain) and then through a memoryless nonlinearity h(.) which satisfies

$$h(z) = \begin{cases} P_0 & \text{for } z \ge \epsilon \\ P_0 z/\epsilon & \text{for } 0 \le z < \epsilon , P_0 < \pi^2 EI/L^2 \\ 0 & \text{for } z < 0 \end{cases}$$
(4.26)

For this feedback connection, we now have the following result:

**Theorem 2:** (Asymptotic Stability of Feedback Connection) The origin of the dynamical system in Figure (4.3) is globally asymptotically stable.

**Proof:** The states of the feedback connection are comprised of the states of the dynamical system in Equation (4.18), namely,  $x_1 \in \mathbb{R}^N$ ,  $x_2 \in \mathbb{R}^N$ , and the state of the low-pass filter,  $z \in \mathbb{R}$ . Let us therefore consider the positive definite radially

unbounded Lyapunov function candidate

$$V_2(x_1, x_2, z) = V_1 + \tau \int_0^z h(\sigma) d\sigma = \frac{1}{2} \left( x_1^T K x_1 + x_2^T x_2 \right) + \tau \int_0^z h(\sigma) d\sigma \quad (4.27)$$

Using Equation (4.22) , the derivative of  $V_2$  is found to be

$$\dot{V}_{2} = -x_{2}^{T} D x_{2} + (x_{2}^{T} C x_{1}) u + \tau h(z) \dot{z}$$

$$= -x_{2}^{T} D x_{2} - y u + h(z) (-z + y)$$

$$= -x_{2}^{T} D x_{2} - z h(z)$$

$$\leq -x_{2}^{T} D x_{2} \leq 0 \tag{4.28a}$$

Since D is positive definite,  $\dot{V}_2 = 0$  implies  $(x_1, x_2, z)$  belongs to the set  $\{x_2 = 0\}$ . In this set,  $y = -x_2^T C x_1 = 0$  which implies  $z \to 0$  as  $t \to \infty$ . This in turn implies u = h(z) = 0. Since  $x_2$  remains identically zero, we can use Equation (4.18) to claim  $x_1 = 0$  and establish that the maximum invariant set in  $\{x_2 = 0\}$  contains only the origin  $(x_1, x_2, z) = (0, 0, 0)$ . Since  $V_2$  is radially unbounded, we can use LaSalle's Theorem [59] to claim global asymptotic stability.  $\diamond \diamond \diamond$ 

Remark 2: The modified control design in Figure (4.3) incorporates a low-pass filter to attenuate high frequency components of  $y = -x_2^T C x_1$ . The bandwidth of the filter can be chosen such that the control input does not exceed the bandwidth of the actuator. The memoryless nonlinearity is incorporated in the control system to guarantee that the control input is always positive since a negative end force cannot be applied by a cable, as in our set up. We repeat the simulation of Section 4.4 to investigate the efficacy of the modified control design. The simulation results are presented in Figure (4.4) for our choice of low-pass filter bandwidth  $\omega_b = 1/\tau = 15$  rad/sec. The results in Figure (4.4) indicate that the modal amplitudes decay slowly

for the control design in Figure (4.3) in comparison to those obtained with the control design in Equation (4.20), shown in Figure (4.2). The control action in Figure (4.4), however, switches less frequently as compared to the control action in Figure (4.3). Clearly, the bandwidth of the filter provides a tradeoff between switching frequency of the control input and speed of vibration suppression. A higher bandwidth (smaller value of  $\tau$ ) results in faster vibration suppression but causes the input to switch very frequently, whereas a lower bandwidth results in less switching of the control input but requires longer time for vibration suppression.

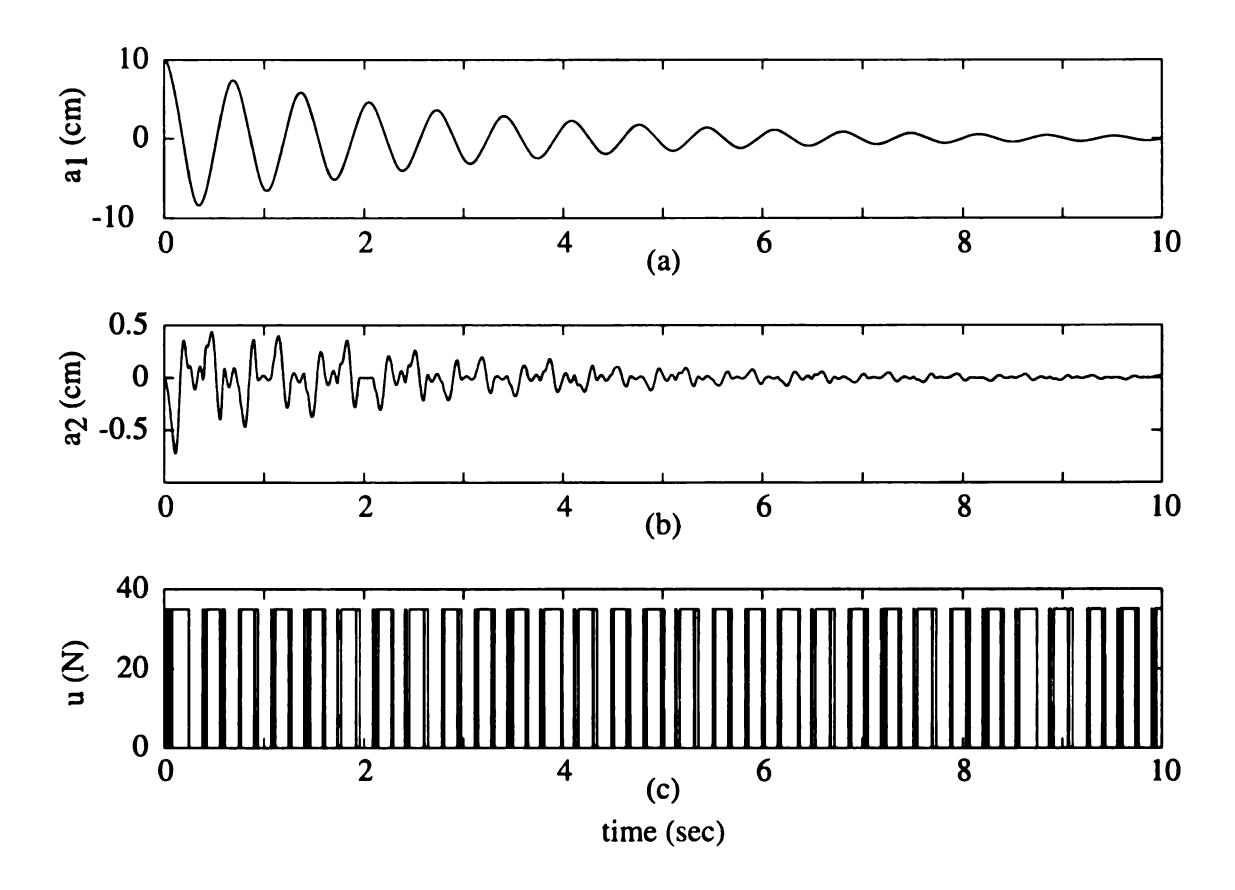


Figure 4.4. Plot of modal amplitudes  $a_1$  and  $a_2$ , and the control action u for the modified control design when  $\epsilon = 0$ .

### 4.6 Adding bias tension in the cable

In general, cables have a certain amount of slack in their state of zero tension. Therefore, an actuator providing the end force in Figure (4.3) will have to first overcome the slack when it switches the tension from zero value to the positive value  $P_0$ . This displacement of the actuator will require finite time and cause delay in switching the end force, which is likely to result in instability. To circumvent this problem, we propose to incorporate bias tension in the cable, as shown in Figure (4.5).

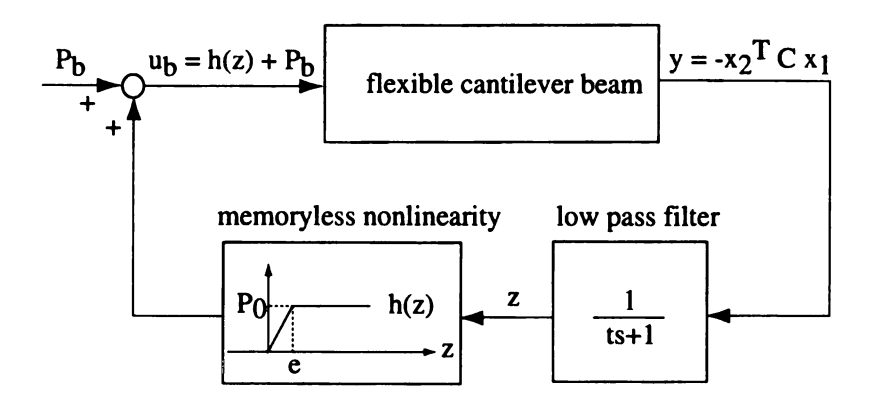


Figure 4.5. Control design based on bias tension and output filtering.

Of course, the bias tension can only be positive and the sum of the bias tension and the controlled tension should not exceed the buckling load for stability, i.e.

$$P_0 > 0, \qquad (P_b + P_0) < \pi^2 EI/L^2$$
 (4.29)

By replacing u in Equation (4.18) with  $u_b = h(z) + P_b$ , as shown in Figure (4.5), the dynamic equations revert to the form

$$\dot{x}_1 = x_2 \tag{4.30a}$$

$$\dot{x}_2 = -\bar{K}x_1 - Dx_2 + Cx_1u, \qquad \bar{K} \triangleq (K - P_bC)$$
 (4.30b)

where  $\bar{K}$  is positive definite since K and C are both positive definite matrices and  $P_b$  is less than the buckling load. We now state a corollary of Theorem 2.

**Corollary 1:** The origin of the dynamical system in Figure (4.5) is globally asymptotically stable.

**Proof:** It is clear from Equation (4.30) that if we replace the beam in Figure (4.3) (with natural frequencies equal to eigenvalues of K) with an identical beam with natural frequencies equal to the eigenvalues of  $\bar{K}$ , Figure (4.5) becomes equivalent to Figure (4.3). Therefore, Theorem 2 can be applied to establish global asymptotic stability of the origin of the dynamic system in Figure (4.5).  $\diamond \diamond \diamond$ 

Remark 3: We know from Corollary 1 that stability of the system is not adversely affected by bias tension. On the contrary, bias tension increases structural damping and results in faster vibration suppression. This will be established in the next section, through experiments.

### 4.7 Experimental verification

### 4.7.1 Hardware description

In our experimental setup, the end force was applied using a Kevlar cable, wrapped around the front face of the beam. The free ends of the cable were wrapped around pulleys fixed to the base of the beam and then tied together to a pulley on a motor shaft. The motor, manufactured by MicroMo Electronics [64], was driven by a power amplifier manufactured by Advanced Motion Control [26], in current mode. A piezo-electric transducer, manufactured by Mide Technology Corporation [57], was used to sense the displacement of the beam. It was placed approximately 0.38 m from the fixed end of the beam wherefrom states  $x_1$  and  $x_2$  corresponding to both the first

and second modes of vibration of the beam are observable.

We programmed our observer-based control law in the Matlab/Simulink $^{TM}$  environment and downloaded it to our dSPACE DSP\* board, not shown in Figure (4.6). The DSP Board resides in our control computer and reads the signal provided by the piezoelectric sensor. This signal is used to estimate the states,  $x_1$ ,  $x_2$  (the observer design is discussed in Section 4.7.3), and compute the signal  $x_2^T C x_1$  (see Figure (4.5)). The signal is filtered and rectified to generate the control action,  $u_b$ . The DSP board provides a reference signal to the power amplifier that is proportional to the control action  $u_b$ ; the proportionality constant depends on the gain of the amplifier, the motor torque constant, and other mechanical parameters of our setup, such as radius of the pulley on the motor shaft.

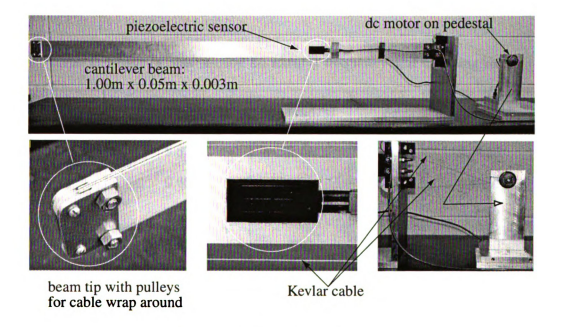


Figure 4.6. Experimental setup

<sup>\*</sup>Digital Signal Processor

### 4.7.2 The effect of bias tension on structural damping

In this section we present experimental data on free vibration of the cantilever beam in the presence of bias tension. The data, provided in Table 1, indicates that the first natural frequency,  $\omega_1$ , decreases, and the damping ratio,  $\zeta$ , increases, with increase in bias tension,  $P_b$ . The first natural frequency computed from our theoretical model,  $\lambda_{min}^{1/2}[K-P_bC]$ , differs slightly from the values obtained experimentally but shows the same trend as  $\omega_1$  and provides confidence in our results. Although  $\omega_1$  decreases and  $\zeta$  increases, the product,  $\zeta\omega_1$ , increases with increase in bias tension. This, evident from the last column of data in Table 1, indicates that structural damping for the first mode increases with increase in bias tension. To the best of our knowledge there has been no studies reported on the variation in structural damping due to variation of end force.

Table 1. Effect of bias tension on natural frequency and damping ratio

$P_b$ (N)	$\lambda_{min}^{1/2}[ar{K}] \; (\mathrm{rad/s})$	$\omega_1 \; ({ m rad/s})$	ζ	$\zeta\omega_1~({ m rad/s})$
0	9.87	9.42	0.0058	0.0546
4	9.65	9.28	0.0070	0.0649
8	9.43	9.13	0.0078	0.0712
12	9.17	9.04	0.0083	0.0750
16	8.88	8.85	0.0085	0.0752
20	8.57	8.70	0.0090	0.0783

The same overall trend has also been observed for the second mode of vibration, i.e., the natural frequency,  $\omega_2$ , decreases, and modal damping,  $\zeta\omega_2$ , increases, with increase in bias tension. We do not provide the results here but would like to comment that the experimental procedures were different for the first and second modes. For

the first mode, the beam was given an initial displacement corresponding to its first mode shape and the data collected from free vibration of the beam. For the second mode, the natural frequency was determined by sinusoidally exciting the piezoelectric transducer attached to the beam and identifying the excitation frequency that causes resonance in the second mode.

### 4.7.3 Observer design

In this section we briefly discuss the procedure adopted for the design of a stable observer. For our observer, we used Equation (4.30) and the output equation

$$\bar{y} = C_1 x, \tag{4.31}$$

where  $C_1^{\dagger}$  can be computed [51] from the dimensions of the piezoelectric sensor and its location on the beam. Since the state equations can be written in the form  $\dot{x} = A(t) x$ ,  $x \triangleq (x_1, x_2)^T$ , the observer is designed as follows

$$\dot{\widehat{x}} = A(t)\widehat{x} + L(\overline{y} - C_1\widehat{x}), \qquad A(t) = \begin{bmatrix} 0 & I \\ -[K - u_b C] & D(u_b) \end{bmatrix}$$
(4.32)

where I is the identity matrix and L is the vector of observer gains. The time dependence of A(t) can be attributed to the fluctuation of  $u_b(t)$  between the values  $P_b$  and  $(P_b + P_0)$ , as well as variation in structural damping due to variation in  $u_b$ . The dependence of structural damping on the end force was mentioned in Remark 3 and conclusively established from experimental data in section 4.7.2. The state variable description in Equation (4.30) and the observer equation in Equation (4.32)

 $<sup>^{\</sup>dagger}C_1$  should not be confused with the positive definite square matrix C in Equation (4.30)

gives us the error equations

$$\dot{e} = [A(t) - LC_1] e \tag{4.33}$$

wherein A(t) fluctuates between the two fixed descriptions

$$A_{1} = \begin{bmatrix} 0 & I \\ -[K - P_{b}C] & D(P_{b}) \end{bmatrix} A_{2} = \begin{bmatrix} 0 & I \\ -[K - (P_{b} + P_{0})C] & D(P_{b} + P_{0}) \end{bmatrix}$$
(4.34)

In equation (4.34), D(.) denotes the functional dependence of D on the end force. Equation (4.33) represents a switched linear system and hence stability of the observer cannot be ensured by simply choosing L that guarantees  $[A_1 - LC_1]$  and  $[A_2 - LC_1]$  are Hurwitz. This is true since switching between two stable systems can potentially result in instability [34] We avoid this problem by designing a high-gain observer [59] where large values of the gains, L, minimize fluctuation in A(t) due to change of the end force.

#### 4.7.4 Results

The voltage output of the piezoelectric sensor provides a measure of the residual vibration in the beam and we plot this voltage to compare vibration attenuation in the presence and absence of control. For proper comparison, we provided the same initial conditions in all our experiments; the beam was deflected purely in its first mode and the initial deflection corresponded to a PZT output of 10 volts.

The plots in Figure (4.7)(a) and (b) depict free vibration of the beam in the absence of bias tension and presence of 20 N bias tension, respectively. These results indicate that structural damping increases due to the application of an end force and supports the data in Table 1. The plots in Figure (4.7) also indicate that vibration is attenuated very slowly in the absence of active control.

The results in Figure (4.8) correspond to active vibration suppression using our

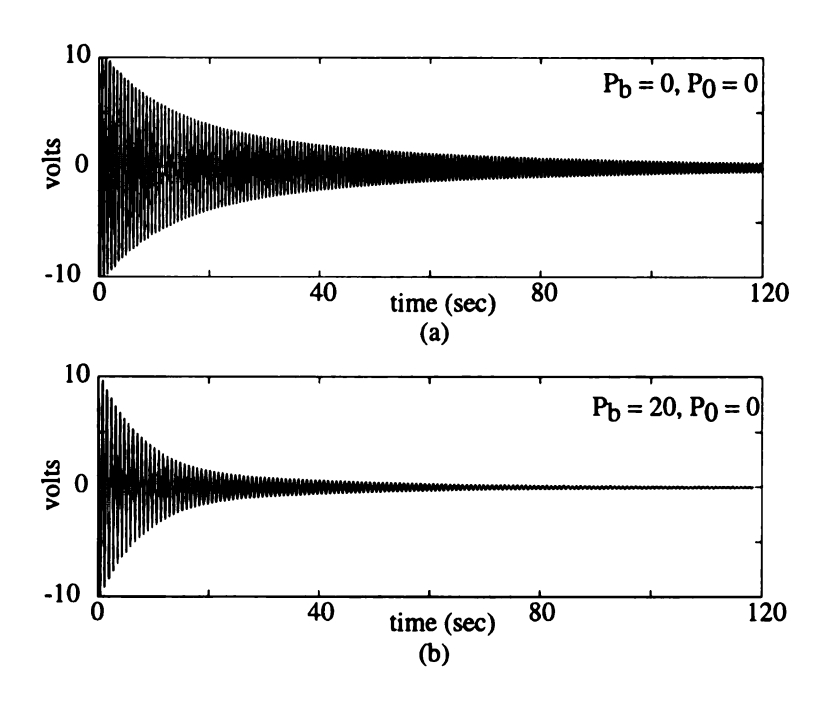


Figure 4.7. Free vibration: (a) in the absence of bias tension, and (b) in the presence of 20 N bias tension

buckling-type end force and two-mode approximation of the beam dynamics. The different plots in Figure (4.7) were obtained with different combinations of bias tension,  $P_b$ , and the maximum control force,  $P_0$ , as shown in Table 4.2. For all three experiments, the value of  $\tau$  was kept fixed at 0.2 secs.

Table 2. Different values of bias tension,  $P_b$ , and maximum control force,  $P_0$ , in experiments with active control

	$P_b$ (N)	$P_0$ (N)
Fig.8(a)	20.0	4.0
Fig.8(b)	20.0	2.0
Fig.8(c)	12.0	4.0

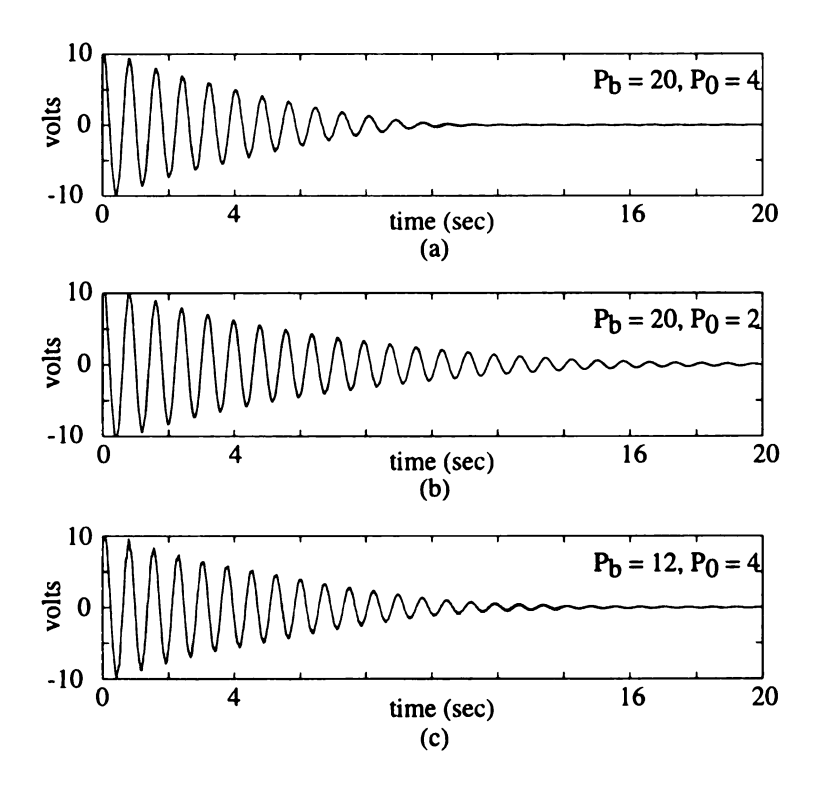


Figure 4.8. Vibration suppression using active control

It is clear from Figure (4.8)(a) and (b) that a larger value of the maximum control force,  $P_0$ , leads to faster vibration suppression. A larger value of  $P_0$  also requires us to change the slope of the saturation function h(.) but we do not discuss this here. A comparison of Figure (4.8)(a) and (c) indicates that a higher value of bias tension,  $P_b$ , leads to faster vibration suppression. This can be attributed to higher structural damping associated with higher bias tension, which was established earlier through experiments. A comparison of the time required for vibration suppression in Figure (4.7) and Figure (4.8) demonstrates the efficacy of our control strategy. We complete this section with one more set of experimental results. These results, which were obtained with a one-mode approximation of the beam dynamics. The results, shown in Figure (4.9), illustrate the role of the low-pass filter in reducing spillover [10]. For both experiments shown in Figure (4.9), we used  $P_b = 8N$  and  $P_0 = 4N$ . The low-pass filter was not used for the experiment in Figure (4.9a) but was used for the

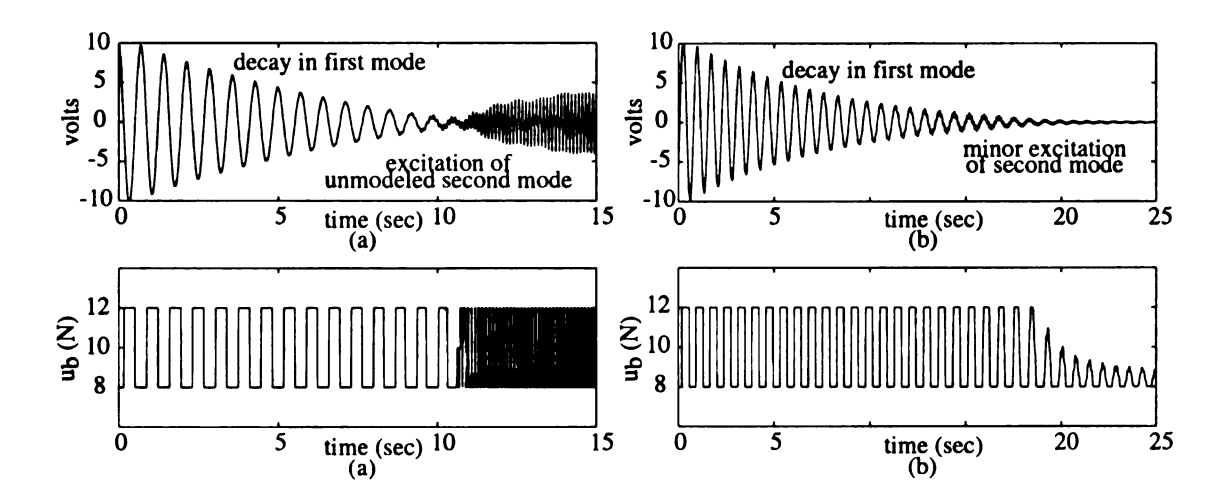


Figure 4.9. Vibration suppression using a one mode dynamic model results a)-spill over problem b)- the role of low pass filter in reducing the effect of spillover

experiment in Figure (4.9b) with  $\tau = 0.2secs$ . From the results in the Figure (4.9), we can make the following observations:

- 1. The modal controllers in both experiments were effective in attenuating vibration associated with the first mode.
- 2. The unmodeled second mode was excited in the experiments corresponding to Figure (4.9a). This phenomenon of spillover [10] was significantly reduced by the low-pass filter in the feedback loop, in the experiment corresponding to Figure (4.9b).
- 3. Although the low-pass filter reduces spillover, it increases the time required for vibration attenuation. This is evident from the experimental results in the Figure (4.9) and corroborates our earlier simulations.

## CHAPTER 5

# **Modal Disparity**

#### 5.1 Background

In this chapter we utilize a buckling-type end force to modify the modal characteristics of a cantilever beam. The objective is to change the mode shapes of the beam and to exploit these changes in control design. Specifically, we vary the frequencies and mode shapes by applying an end load, and by switching between different sets of modal characteristics, funnel energy from the higher modes to the lower modes. The energy associated with the lower modes can then be dissipated by employing a low dimensional state space model. The success of this strategy relies on the difference in modal characteristics under different levels of end loads, which we refer to as *modal disparity*.

#### 5.2 Proof of concept

Consider the cantilever beam with a buckling type end force studied in Chapter 4. For different levels of the end load, the mode shapes of the beam can be determined

using Equation (4.15). For this purpose we do a coordinate transformation as follows

$$a = [T]z \tag{5.1}$$

where columns of [T], the transformation matrix, are formed using eigenvectors of [K] - P[C]. Substituting for a from Equation (5.1) into Equation (4.15) results

$$\ddot{z} + [\Omega]z = 0 \tag{5.2}$$

where  $[\Omega] = [T]^{-1}([K] - P[C])[T]$ . In this equation  $[\Omega]$  is a diagonal matrix consists of squared of natural frequencies of the beam. Now, plugging for a from Equation (5.1) in Equation (4.13), results

$$y_N(x,t) = z^T [T]^T \phi = \sum_{i=1}^N z_i(t) \, \psi_i(x)$$
 (5.3)

in which  $\psi = [T]^T \phi$  are the true mode shapes of the beam. For P = 40N the mode shapes are shown in Figure (5.1) and compared with those with P = 0. From the figure it is clear that the application of the end load changes the mode shapes. Now, consider an idealized static problem wherein the end-force is instantaneously switched between two values 0 and  $P_0$ , and the fundamental modal components are repeatedly removed from the system after each switch. We will show that such a strategy removes energy from the beam, including higher mode, in a systematic manner, and requires that one be able to control the fundamental mode corresponding to the free beam and the beam with end load  $P_0$ . For the calculations we denote the attendant mode shapes for the free beam and the beam with end load  $P_0$  as  $\phi_j(x)$  and  $\psi_j(x)$ , respectively. If one starts with a beam deflection  $y_0(x,t)$  and no end-load,

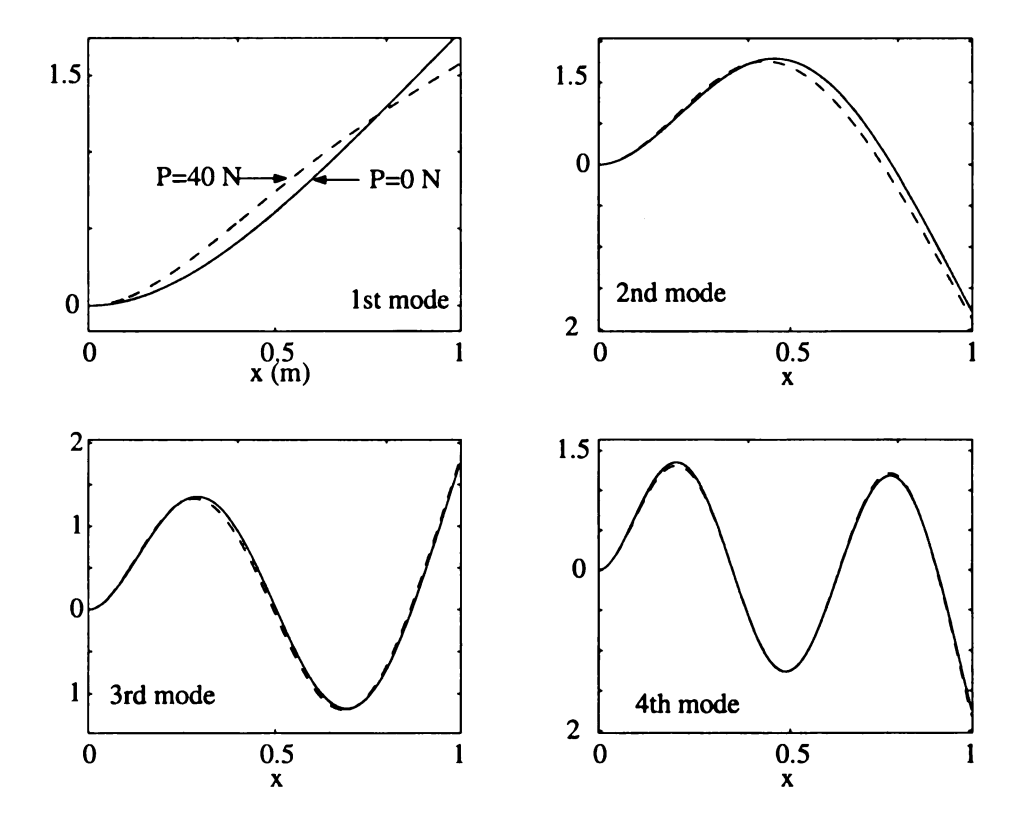


Figure 5.1. cantilever beam mode shapes for P = 0 and P = 40N

then we can write

$$y_0(x,t) = \sum_{j=1}^{N} \delta_j(t)\phi_j(x)$$
 (5.4)

where N denotes the modal truncation level and  $\delta_j(t)$ s are the modal amplitude components. Assuming that one can remove the first mode, the resulting shape is given by

$$y_1(x,t) = y_0(x,t) - \delta_1(t)\phi_1(x) = \sum_{j=2}^{N} \delta_j(t)\phi_j(x)$$
 (5.5)

At this point the end-load is switched to  $P_0$  and the shape is now conveniently expressed as

$$y_1(x,t) = \sum_{j=1}^{N} \beta_j(t) \psi_j(x)$$
 (5.6)

It is assumed that the first mode again removed while  $P = P_0$ , resulting in the shape

$$y_2(x,t) = \sum_{j=2}^{N} \beta_j(t)\psi_j(x)$$
 (5.7)

The end-load is then switched back to 0 where the shape can then be expressed by

$$y_2(x,t) = \sum_{j=1}^{N} \gamma_j(t)\phi_j(x)$$
 (5.8)

This completes one cycle of the process, and one is interested in how the new modal coefficients, the  $\gamma_j(t)$ s are related to the originals, the  $\delta_j(t)$ s. This is conveniently described by a linear mapping

$$\Gamma = M\Delta \tag{5.9}$$

where  $\Gamma$  and  $\Delta$  are the vectors of modal coefficients.

$$\Gamma = (\gamma_1, \, \gamma_2, \, \dots, \, \gamma_n)^T \tag{5.10}$$

$$\Delta = (\delta_1, \, \delta_2, \, \dots, \, \, \delta_n)^T \tag{5.11}$$

and M, the mapping matrix, can be developed by a sequence of calculations that use modal projections for each level of the end- force as follows

$$\gamma_i(t) = \langle y_2(x,t), \phi_i(x) \rangle = \langle \sum_{j=2}^N \beta_j(t) \psi_j(x), \phi_i(x) \rangle = \sum_{j=2}^N \beta_j(t) \langle \psi_j(x), \phi_i(x) \rangle$$
 (5.12)

and similarly

$$\beta_j(t) = \sum_{k=2}^{N} \delta_k(t) \langle \psi_j(x), \phi_k(x) \rangle^*.$$
 (5.13)

 $<sup>^*\</sup>langle f,g
angle$  is the inner product of functions f and g denoted by  $\int_0^L fg\,dx$ 

Now, Substituting for  $\beta_j(t)$  from Equation (5.13) in Equation (5.12), results

$$\gamma_i(t) = \sum_{j=2}^{N} \sum_{k=2}^{N} \langle \phi_i(x), \psi_j(x) \rangle \langle \psi_j(x), \phi_k(x) \rangle \delta_k, \quad i = 1, ..., N$$
 (5.14)

Comparing this equation with Equation (5.9), reveals that the structure of the mapping matrix M. It should be noticed the convergence of this process depends on the  $N \times N$  linear operator M, which can be constructed as follows: the first column contains all zeros since the first modal coefficient was zeroed out (note that this implies that M will always have at least one zero eigenvalues). The remaining columns are filled in by the coefficient  $\langle \phi_i(x), \psi_j(x) \rangle \langle \psi_j(x), \phi_k(x) \rangle$ ,  $i=1,2,...,N, \ k=2,3,...,N$ . If all eigenvalues of M lie inside the unit circle, the process will converge, implying that all modes consideration die out under repeated cycling and removal of the first relevant mode. In fact rate of convergence (or divergence) is dictated by these eigenvalues. For better understanding, in Figure (5.2) a schematic of the concept of the modal disparity is depicted.

As an example, the cantilever beam studied in Chapter 4 is used to demonstrate the methodology for  $P_0 = 40N$ . For this case the eigenvalues of the mapping matrix M is

$$\lambda_i = \{0, 0.51, 0.87, 0.92\} \tag{5.15}$$

We can see that the eigenvalues corresponding to the higher modes is close to unity. This implies that the rate of convergence for the higher modes will be smaller compared to the lower modes. In this calculation it is assumed that the end-force does not add or remove energy to or from the beam in the time interval that is switched on, which is very unlikely. In the next section we will consider the effect of switching on the total energy of the beam by investigating the subsystems corresponding to different levels of the end load.

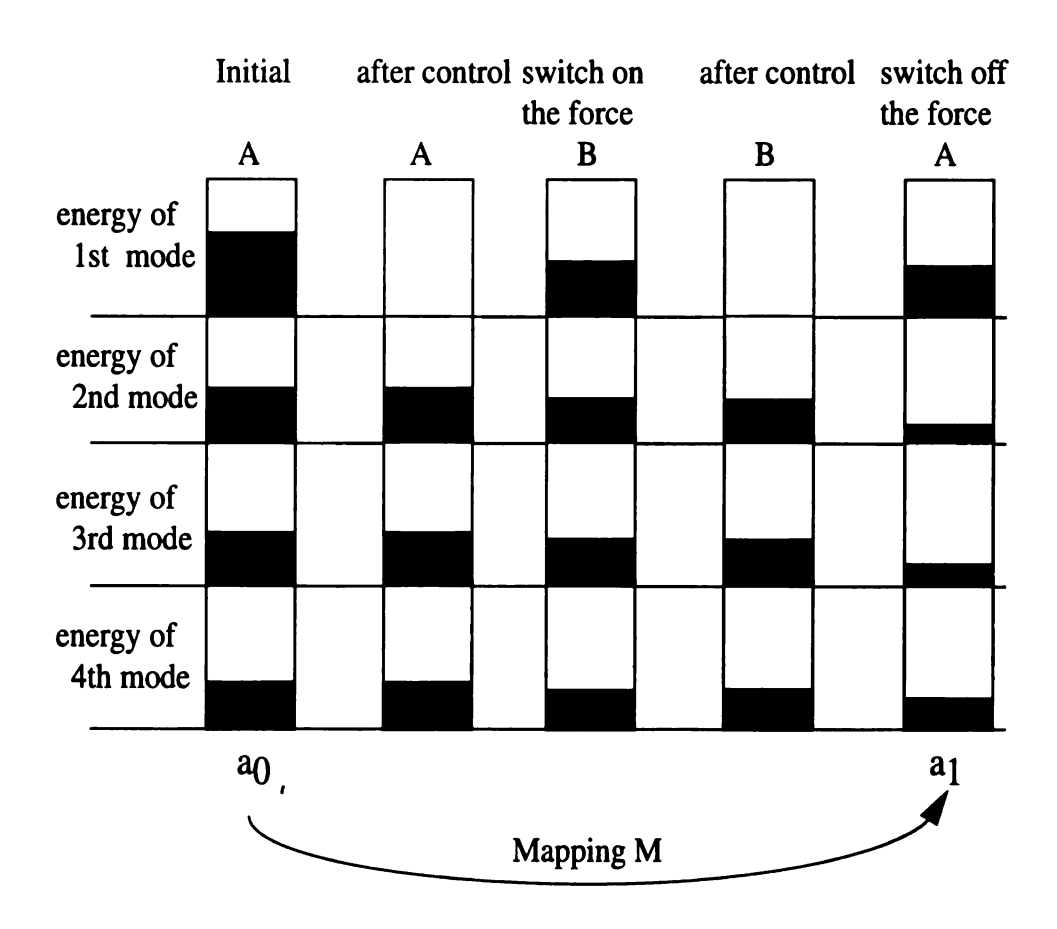


Figure 5.2. Concept of the modal disparity

#### 5.3 Dynamic analysis

From Equation (4.17) in Chapter 4, we have the following mathematical model for the beam subjected to the end load P

$$\{\ddot{\delta}\} + [D]\{\dot{\delta}\} + ([K]_{n \times n} - P[C]_{n \times n})\{\delta\} + H_1(\delta_1, \dot{\delta_1}) = 0$$
 (5.16)

where P is always less than  $P_{buckling}$ . In this equation [D] is the diagonal modal damping matrix, assumed to be constant, and  $H_1$  is the vector of control laws corresponding to the different modal coordinates. All the enterers of  $H_1$  are zero except the first, which is assumed to be  $h_1$ . Our goal here is to design a switching strategy

for the end force to transfer energy of the higher modes to the first mode such that it can be subsequently dissipated by the control law  $h_1$ . We expand Equation (5.16) as follows

$$\dot{\delta_{1}} + D_{11}\dot{\delta_{1}} + K_{11}\delta_{1} + h_{1}(\delta_{1}, \dot{\delta_{1}}) = P[C_{1}]_{1 \times n} \{\delta\}$$

$$\dot{\delta_{2}} + D_{22}\dot{\delta_{2}} + K_{22}\delta_{2} = P[C_{2}]_{1 \times n} \{\delta\}$$

$$\vdots$$

$$\dot{\delta_{n}} + D_{nn}\dot{\delta_{n}} + K_{nn}\delta_{n} = P[C_{n}]_{1 \times n} \{\delta\}$$
(5.17a)

In the above equation  $D_{ii}$  is the  $i^{th}$  diagonal element of the [D] matrix and  $[C_i]$  refers to the  $i^{th}$  row of the [C] matrix. By multiplying the first row of Equation (5.17) by  $\dot{\delta_1}$ , the second row by  $\dot{\delta_2}$ , and so on, we get

$$\begin{cases}
\dot{E}_{1} = -\dot{\delta}_{1}D_{11}\dot{\delta}_{1} - \dot{\delta}_{1}h_{1}(\dot{\delta}_{1}, \delta_{1}) + Pw_{1}(\dot{\delta}_{1}, \delta) \\
\dot{E}_{2} = -\dot{\delta}_{2}D_{22}\dot{\delta}_{2} + Pw_{2}(\dot{\delta}_{2}, \delta) \\
\vdots \\
\dot{E}_{n} = -\dot{\delta}_{n}D_{nn}\dot{\delta}_{n} + Pw_{n}(\dot{\delta}_{n}, \delta)
\end{cases} (5.18)$$

where  $E_i = \frac{1}{2}(\dot{\delta}_i^2 + K_{ii}\delta_i^2)$ , is the modal energy corresponding to the  $i^{th}$  mode and  $w_i(\dot{\delta}_i, \delta) = \dot{\delta}_i[C_i]\delta$ .

Summing up all the rows of this equation, results in

$$\frac{d}{dt}(E_1 + E_2 + \dots + E_n) = -\sum_{i=1}^n \dot{\delta}_i D_{ii} \dot{\delta}_i + P \sum_{i=1}^n w_i (\dot{\delta}_i, \delta) - \dot{\delta}_1 h_1 (\dot{\delta}_1, \delta_1)$$
 (5.19)

The first term at the right hand side of Equation (5.19) is negative definite whereas the third term can be made negative semi definite. The second term can be made negative definite if we apply the end load when  $\sum_{i=1}^{n} w_i(\dot{\delta_i}, \delta)$  is negative. This would constitute the approach taken in Chapter 4. In order to clearly illustrate the concept

of modal disparity, one can design a switching strategy such that the end load does not change the overall energy of the system. This can be done, for example, if we apply the end load over any interval in which  $\int (\sum_{i=1}^n w_i(\dot{\delta}_i, \delta)) = 0$ .

We now present a simulation that combines the approach of Chapters 4 and that of modal disparity. In this combined approach, we design the switching strategy such that the end load reduces the over all energy of the system (approach of Chapter 4) as well as funnels energy from the higher modes to the first mode (approach based on the concept of modal disparity). This switching strategy can be chosen as follows:

a) apply end load when the following conditions are satisfied

$$\begin{cases} w_1 > 0 \\ & \& \\ w_1 + w_2 + \ldots + w_n < 0 \end{cases}$$
 (5.20)

b) remove end load otherwise.

In the next section we provide a numerical simulation to illustrate this approach.

#### 5.4 Numerical example

In our simulation we assume the material and geometric properties of the beam as follows:

Material Aluminum

Young's modulus 70 GPa

Mass density  $2730 \text{ kg/m}^3$ 

Dimensions  $1.00 \times 0.05 \times 0.003 \text{ m}$ 

A four-mode approximation of the beam dynamics is considered. To better illustrate energy dissipation by the end load as well as energy transfer from the higher modes to the first mode due to the end load, we assume modal damping to be absent. For the same reason, we do not remove the energy of the first mode and therefore choose the control law *i.e.*  $h_1(\delta, \dot{\delta}_1) = 0$ . The simulation results are shown in Figure (5.3) for the following initial conditions

$$x(0) = [1, -1, -0.5, 0.5]$$
 (5.21a)

$$\dot{x}(0) = [0, 0, 0, 0] \tag{5.21b}$$

and  $P_0$  is equal to 40 N.

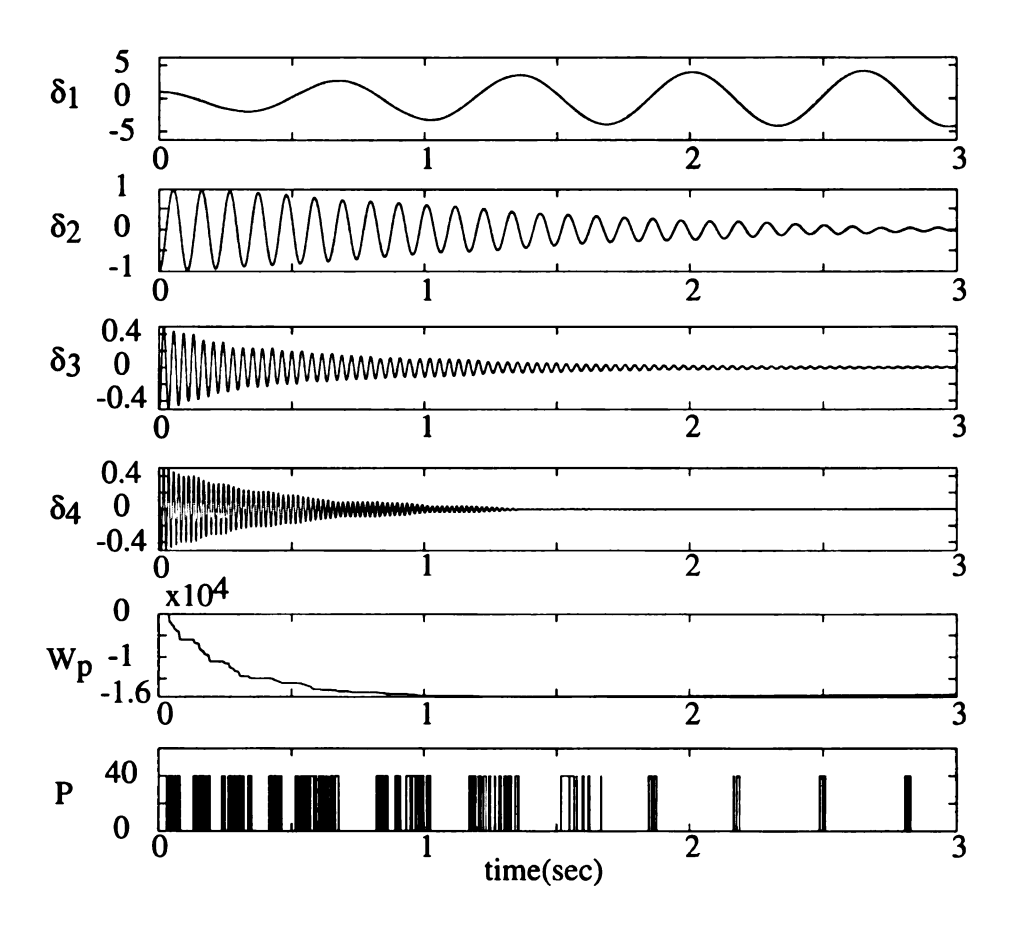


Figure 5.3. plot of the modal amplitude for the described switching strategy in Equation (5.20)

In Figure (5.3) the first four plots show the amplitude of first four modes, respectively. The fifth plot shows the work done by the end-force and the last plot is the time history of the end load. As we can seen in this simulation, amplitude of the first mode increases. This indicates that some of the energy associated with the higher modes is pumped into the first mode and consequently the amplitude of the second, third and the fourth modes decrease. In fact, decrement in the amplitude of the higher modes occurs for two reasons: first, their energy is funnelled to the first mode, and second, the end load is doing negative work.

The main concern regarding this simulation is that the end load needs to switch on and off quite rapidly. This implies that if the actuator does not have the requisite bandwidth, the switching will not occur at the right time and this can result in energy being pumped into the system. One way to circumvent the requirement of high actuator bandwidth is to discard the high frequency components of  $w_2 + \ldots + w_n$  using a low pass filter in the loop that is described in the next section.

#### 5.5 Modified switching strategy

We propose the control system block diagram in Figure (??) to reduce the actuator bandwidth requirement.

In this diagram,  $h_1(z)$  and  $h_2(w)$  are two memoryless nonlinearities described below

$$h_1(z) = \begin{cases} P_0 & \text{for } z > 0 \\ 0 & \text{for } z \le 0 \end{cases} \qquad h_2(w) = \begin{cases} 1 & \text{for } w > 0 \\ 0 & \text{for } w \le 0 \end{cases}$$
 (5.22)

To reduce the speed of switching of the end force, we remove the high frequency components of  $w_i$  by feeding the signal through a low pass filter (of time constant  $\tau$  and unity DC gain) and then through the memory less nonlinearity  $h_1(.)$ .

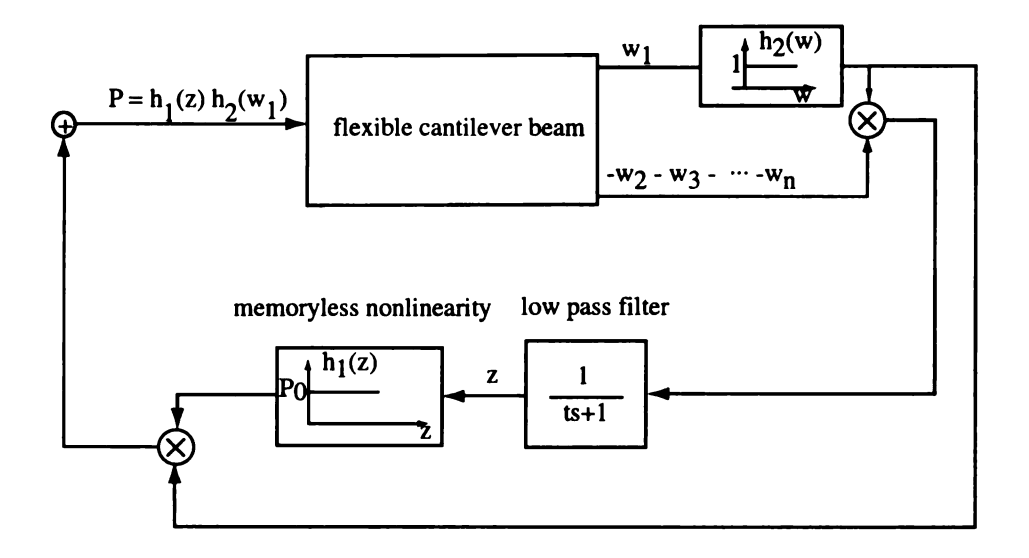


Figure 5.4. Modified switching strategy

To prove that the energy associated with the higher modes decreases, we look at the time derivative of the following Lyapunov function [59]

$$E_{total} = E_2 + E_3 + \ldots + \tau \int_0^z h_1(\sigma) d\sigma$$
 (5.23)

where,  $E_{total}$  consists of two positive terms, namely, energy of the second and higher modes and the area under the positive function  $h_1(z)$ . From Equation (5.19) we have

$$\frac{dE_{total}}{dt} = -\sum_{i=2}^{n} \dot{\delta}_i D_{ii} \dot{\delta}_i + P \sum_{i=2}^{n} w_i (\dot{\delta}_i, \delta) + \tau \dot{z} h_1(z), \tag{5.24}$$

Using Figure (5.4), we can say

$$\frac{dE_{total}}{dt} = -\sum_{i=2}^{n} \dot{\delta_i} D_{ii} \dot{\delta_i} + P \sum_{i=2}^{n} w_i (\dot{\delta_i}, \delta) + h_1(z) \left( -z - h_2(w_1) \sum_{i=2}^{n} w_i (\dot{\delta_i}, \delta) \right)$$
(5.25)

where

$$P = h_1(z)h_2(w_1) (5.26)$$

Therefore, we have

$$\frac{dE_{total}}{dt} = -\sum_{i=2}^{n} \dot{\delta}_{i} D_{ii} \dot{\delta}_{i} - z h_{1}(z)$$
(5.27)

Using LaSalle's Theorem [59] and the analysis similar to that used in Chapter 4, we can claim asymptotic stability of the origin. Hence, the energy of the higher modes will eventually decay to zero.

We repeat the previous simulation to investigate the usefulness of the modified switching strategy. In this simulation we assume small value for modal damping. The control law for removing oscillations of the fundamental frequency is considered absent. The simulation results are presented in Figure (5.5) for our choice of low pass filter bandwidth of  $\omega_b = 1/\tau = 50 \ rad/sec$ .

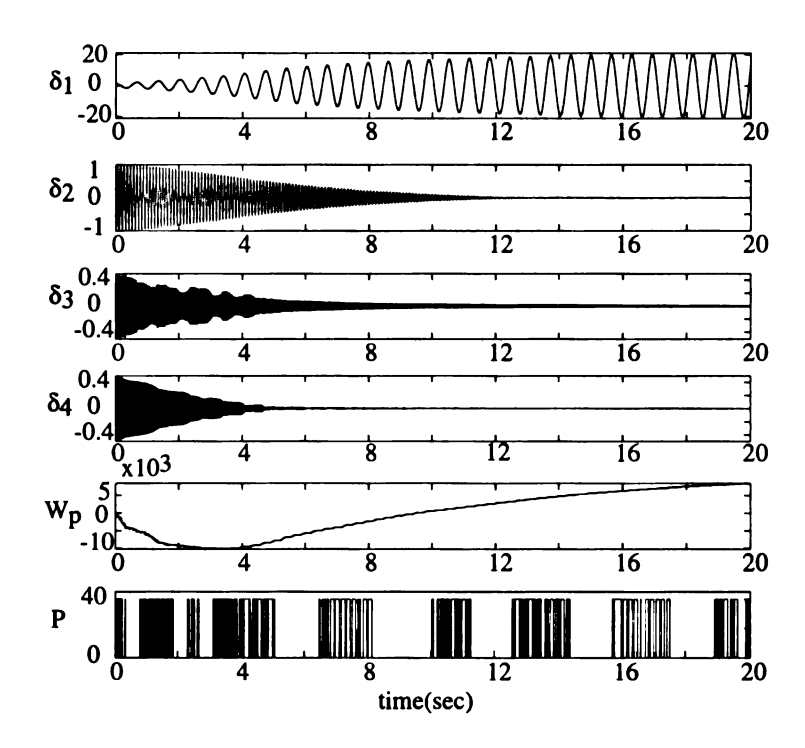


Figure 5.5. Plot of the modal amplitude and the end-force in the presence of the low pass filter in the loop

These results indicate that the modal amplitudes of the higher modes decay slowly in this case as compared to that shown in Figure (5.4). However, in this case the endforce switches less frequently as compared to that shown in Figure (5.3). Clearly, the bandwidth of the filter provides a trade off between switching frequency of the endforce and the effectiveness of the end force in vibration suppression and modal energy redistribution. A higher bandwidth (smaller value of  $\tau$ ) results in faster vibration suppression and higher modal energy redistribution but causes the force to switch very frequently, whereas a lower bandwidth results in less switching of the force but requires longer time for vibration suppression.

Figure (5.4) also shows that when time is less than 10 sec, the work done by the end-force is negative and in next 10 sec, force starts doing positive work. This clearly indicates that the choice of the controller is very important to avoid instability of the first mode. If the controller associated with the first mode can not reject energy that is being pumped by the end-force fast enough, the amplitude of the first mode will keep growing that is not desirable. We show the result of another simulation where an observer-based controller is utilized to remove modal energy of the first mode as well. This controller, chosen as

$$h_1(\dot{\delta_1}, \delta_1) = 3\dot{\delta_1} \tag{5.28}$$

adds damping to the first mode for energy removal. The simulation results for this case is shown in Figure (5.6). In this simulation the initial conditions and low pass filter are the same as the previous simulation. The amplitudes of all modes decay to zero, as expected.

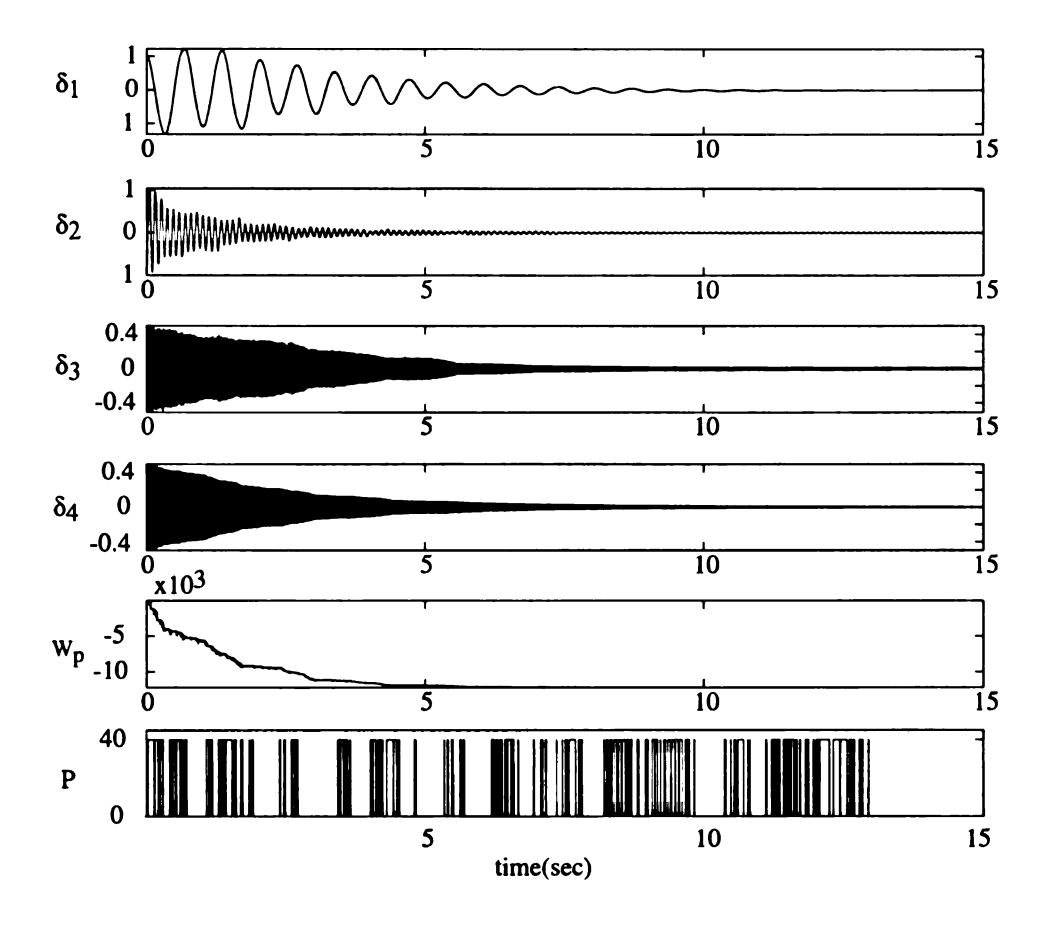


Figure 5.6. Plot of the modal amplitude and the end-force in the presence of the low pass filter and first order controller in the loop

#### 5.6 Experimental Results

For a proof of principal, we conducted two simple experiments with a cantilever beam and an end force. The beam is the same as that used in our experiments in Chapter 4. The end force was applied by the cable and motor mechanism described in Chapter 4. In our experiments, we used a piezoelectric actuator to excite the beam at its natural frequencies. For this purpose, we input the piezoelectric actuator with a sinusoidal signal at the same frequency as the natural frequency of the beam. The beam was excited at its second natural frequency in the first experiment, and its first natural frequency in the second experiment. After excitation of the beam we disconnected

the input to the piezoelectric actuator and applied the end force by energizing the DC motor.

In the first experiments, the oscillations of the beam prior to application of the end force consists only the second mode but consists of both the first and second modes after application of the end force. Clearly, the end force causes energy associated with the second mode to be redistributed among the first and second modes of the modified (beam with non-zero end force) system. The results in the second experiment are also similar; in this case, energy associated with the first mode is redistributed among the first and second modes of the modified system.

The natural frequencies of the beam were not very low and as a result the vibrations decay out rapidly in the presence of damping. The beam is therefore not an ideal experimental platform for demonstration of modal disparity. An ideal platform would be required to have low natural frequencies of vibration, as in the case of large space structures to which this control methodology is targeted.

### CHAPTER 6

### Conclusion

We developed three new control methodologies for vibration suppression of flexible structures. Our main objective was to reduce control system hardware that will in turn reduce the cost and weight of the overall system. This has significant benefits for space applications from cost, weight, and payload considerations.

Our first control methodology, presented in Chapter 3, is based on continuous switching of piezoelectric transducers between actuator and sensor modes. In Chapter 3 we first showed that it is possible to continuously reverse the roles of actuator and sensor transducers in specific dynamical systems to significantly reduce the total number of transducers and the weight and cost of the system without any loss in controllability and observability. We adopted this idea to design an observer-based controller for suppressing vibration in under-actuated and under-sensed Euler-Bernoulli beams. Using simulations, we first demonstrated vibration suppression in first four modes of a flexible beam whose actuator and sensor configurations individually do not provide complete controllability and observability. Our experiments were less extensive than simulations but they sufficiently demonstrated feasibility of controllability and observability enhancement through switching. In our experiments, vibration of the first two modes of a cantilever beam were suppressed using a single piezoelectric transducer, switching between actuator and sensor modes. In general, switching

generates discontinuous control inputs which can excite unmodeled dynamics of a system. This was observed in our experiments where higher unmodeled modes of the beam were excited when we used a fixed-time switching schedule. The problem was remedied by adopting a variable-time switching schedule which generates continuous inputs. We also addressed the problem of optimal switching for faster vibration suppression. For a fixed number of switchings, we determined the optimal switching times apriori, and demonstrated improved performance through experiments.

Our second control methodology for vibration suppression, presented in Chapter 4, is based on the choice of piezoelectric transducers as sensors and motor-driven cable actuators. Although the idea is quite general and is applicable to large structures, we restricted or analysis and experiments to a simple cantilever beam. We demonstrated the use of a compressive buckling-type end load in active vibration control of a cantilever beam. The control process involves the use of piezoelectric transducers for vibration measurements of the beam, an observer to estimate modal vibration amplitudes of the beam, filtering the data to restrict the bandwidth requirement of the cable actuator, and switching the cable actuator on and off to remove the vibration energy of the beam. The stability of the control system is established mathematically and both simulation and experimental results are provided for verification of the theoretical results. The main limitation of this approach is that the number of modes that can be handled is restricted by the bandwidth of the actuator, and hence one can actively control only those modes below a certain frequency threshold. The main advantage of the approach is that all modes below this threshold can be controlled by a single actuator, at least in the particular case of the cantilever beam. The low-pass filter in the feedback loop sidesteps the spillover problem while maintaining stability. However, it adversely affects the settling time of the controlled system and therefore the use of high-bandwidth actuators is desirable. The controller is more effective when both the level of the bias load and the magnitude of the control force

are increased. Of course, this has a limitation, due to the fact that the sum of these forces must remain below the structural buckling threshold.

The third control methodology is described in Chapter 5. In this chapter, we introduce the concept of *modal disparity*. Modal disparity is a measure of the difference between modes in two stiffness states and can be exploited to gain control authority over the significant flexible modes of a system using a low dimensional state space model. In our study, the control methodology relies on variation in stiffness of the beam to achieve modal energy redistribution from higher modes to the lower modes and dissipating the energy associated with the lower modes. Since the lower modes are only estimated and controlled, this approach has the potential to sidestep spillover problem. We present an analytical framework for control design exploiting the concept of modal disparity and verify the results through simulations and very simple experiments.

#### **BIBLIOGRAPHY**

- [1] T. E. Alberts and J. A. Colvin, "Observations on the nature of transfer functions for control of piezoelectric laminates," *Journal of Intelligent Material Systems and Structures*, vol. 8, no. 5, pp. 605-611, 1991.
- [2] T. E. Alberts, T. V. DuBois, and H. R. Pota, "Experimental verification of transfer functions for a slewing piezoelectric laminate beam," Control Engineering Practice, vol. 3, no. 2, pp. 163-170, 1995.
- [3] C. R. Fuller, S. J. Eliott, and P. A. Nelson, *Active Control of Vibration*. Academic Press, New York, NY, 1996.
- [4] R. L. Clark, W. R. Saunders, and G. P. Gibbs, Adaptive Structures: Dynamics and Control. Wiley, NY, 1998.
- [5] E. F. Rawley and J. de Luis, "Use of piezoelectric actuators as elements of intelligent structures," AIAA Journal, pp. 1373-1385, 1987.
- [6] N. W. Hagood, W. H. Chung, and A. von Flotow
- [7] E. D. Garcia, D. Inman, and J. Dosch, "Vibration suppression using smart structures," *Proc. Smart Structures and Materials*, pp. 167–172, 1991.
- [8] K. B. Lazarus, E. F. Crawley, and J. D. Bohlman, "Static aeroelastic control using strained actuated adaptive structures," *Journal of Intelligent Material Systems and Structures*, vol. 2, no. 3, pp. 386–440, 1991.
- [9] R. E. Skelton, "Robust control of aerospace systems," Proc. IFAC Symposium on Robust Control Design, Rio de Janiro, Brazil, 1994.
- [10] M. J. Balas, "Active control of flexible systems," Journal of Optimization Theory and Applications, vol. 25, no. 3, pp. 415-436, 1978.
- [11] M. J. Balas, "Feedback control of flexible systems," IEEE Transactions on Automatic Control, vol. 23, no. 4, pp. 673-679, 1978.

- [12] D. Halim and S. O. R. Moheimani, "Spatial resonant control of flexible sructures

   application to a piezoelectric laminate beam," *IEEE Transactions on Control Systems Technology*, vol. 9, pp. 37–53, 2001.
- [13] E. H. Anderson, N. W. Hagood, and J. M. Goodliffe, "Self-sensing piezo-electric actuation: Analysis and application to controlled structures," *Proc.* AIAA/ASME/ASCE/AHS Structures, Structural Dynamics, Materials Conference, Dallas, TX, pp. 2141–2155, 1992.
- [14] J. J. Dosch, D. J. Inman, and E. Garcia, "A self-sensing piezoelectric actuator for collocated control," *Journal of Intelligent Materials, Systems, and Structures*, vol. 3, no. 1, pp. 166–185, 1992.
- "A [15] J. Holterman and Α. de Vries, comparison of passive methods elements," and active damping based on piezoelectric http://www.ce.utwente.nl/rtweb/publications/2001/pdf-files/034R2001.pdf, 2001.
- [16] D. G. Cole and R. L. Clark, "Adaptive compensation of piezoelectric sensoriactuators," *Journal of Intelligent Material Systems and Strutures*, vol. 5, pp. 665– 672, 1994.
- [17] S. Acrabelli and A. Tonoli, "System properties of flexible structures with self-sensing piezoelectric transducers," *Journal of Sound and Vibration*, vol. 235, no. 1, pp. 1–23, 2000.
- [18] S. O. R. Moheimani, "A survey of recent innovations in vibration damping and control using shunted piezoelectric transducers," *IEEE Transactions on Control* Systems Technology, vol. 11, no. 4, pp. 482-494, 2003.
- [19] M. A. Demetriou, "Numerical algorithm for the optimal placement of actuators and sensors for flexible structures," *Proc. American Control Conference*, pp. 2290–2294, 2000.
- [20] M. Murugavel, "Implementation of an actuator placement switching algorithm for active vibration control in flexible structures," MS Thesis, Department of Mechanical Engineering, Worcester Polytechnic Institute, 2002.
- [21] V. V. Bolotin, Nonconservative Problems of the Theory of Elastic Stability. Pergamon Press, New York, 1963.

- [22] G. Herrmann, "Dynamics and stability of mechanical systems with follower forces," NASA Contractor Report, NASA CR-1782, 1971.
- [23] K. Higuchi and E. H. Dowell, "Dynamic stability of a completely free plate subjected to a controlled non-conservative follower force," *Journal of Sound and Vibration*, vol. 132, no. 1, pp. 115–128, 1989.
- [24] D. H. Hodges, M. J. Patil, and S. Chae, "Effect of thrust on bending-torsion flutter of wings," *Journal of Aircraft*, vol. 39, no. 2, pp. 371–376, 2002.
- [25] M. A. Langthjem and Y. Sugiyama, "Dynamic stability of columns subjected to follower loads: A survey," *Journal of Sound and Vibration*, vol. 328, no. 5, pp. 809–851, 2000.
- [26] O. M. O'Reilly, N. K. Malhotra, and N. S. Namachchivaya, "Some aspects of destabilization of the equilibria of reversible dynamical systems with application to follower forces," *Nonlinear Dynamics*, vol. 10, no. 1, pp. 63–87, 1996.
- [27] S. H. Park and J. H. Kim, "Dynamic stability of a completely free circular cylindrical shell subjected to a follower force," *Journal of Sound and Vibration*, vol. 231, no. 4, pp. 989–1005, 2000.
- [28] Q. H. Zuo and H. L. Schreyer, "Flutter and divergence instability of nonconservative beams and plates," *International Journal of Solids and Structures*, vol. 33, no. 9, pp. 1355–1367, 1996.
- [29] Y. Achkire and A. Preumont, "Active tendon control of cable-stayed bridges," Earthquake Engineering and Structural Dynamics, vol. 25, pp. 585-597, 1996.
- [30] A. Preumont and F. Bossens, "Active tendon control of vibration of truss structures: Theory and experiments," *Journal of Intelligent Material Systems and Structures*, vol. 11, pp. 91–99, 2000.
- [31] G. R. Skidmore and H. J. W. L., "Modal-space active damping of a beam-cable structure: Theory and experiment," *Journal of Sound and Vibration*, vol. 101, no. 2, pp. 149–160, 1985.
- [32] M. E. Magana, P. Volz, and T. Miller, "Nonlinear decentralized control of a flexible cable-stayed beam structure," ASME Journal of Vibration and Acoustics, vol. 119, pp. 523–526, 1997.

- [33] P. Thomson, G. J. Balas, and P. H. Leo, "The use of shape memory alloys for passive structural damping," *Smart Materials and Structures*, vol. 4, pp. 36–42, 1995.
- [34] D. Liberzon and A. S. Morse, "Basic problems in stability and design of switched systems," *IEEE Control Systems Magazine*, vol. 19, no. 5, pp. 59–70, 1999.
- [35] D. Liberzon, J. Hespanha, and A. S. Morse, "Stability of switched systems: A lie algebraic condition," System and Control Letters, vol. 37, pp. 117–122, 1999.
- [36] A. Agrachev and D. Liberzon, "Lie-algebraic stability criteria for switched systems," SIAM Journal of Control and Optimization, vol. 40, no. 1, pp. 253-269, 2001.
- [37] J. Hespanha, "Extending lasalle's invariance principle to switched linearsystems," *Proc.* 40th IEEE International Conference on Decision and Control, pp. 2496–2501, 2001.
- [38] R. DeCarlo, M. Branicky, S. Pettersson, and B. Lennartson, "Perspectives and results on stability and stabilizability of hybrid systems," *Proc. of IEEE*, vol. 88, no. 7, pp. 1069–1082, 2000.
- [39] S. S. Ge, T. H. Lee, and S. Zhendong, "Controllability and reachability criteria for switched linear systems," *Automatica*, vol. 38, no. 5, pp. 775–786, 2002.
- [40] Y. Zhenyu, "An algebraic approach towards the controllability of controlled switching linear hybrid systems," *Automatica*, vol. 38, no. 7, pp. 1221–1228, 2002.
- [41] M. Egerstedt and V. D. Blondel, "How hard is it to control switched systems?," *Proc. American Control Conference*, pp. 1869–1873, 2002.
- [42] M. Branicky, V. Borkar, and S. Mitter, "A unified framework for hybrid control: Model and optimal control theory," *IEEE Transactions on Automatic Control*, vol. 43, no. 1, pp. 31–45, 1995.
- [43] M. Branicky and S. Mitter, "Algorithms for optimal hybrid control," *Proc. 34th IEEE International Conference on Decision and Control*, pp. 2661–2666, 1995.
- [44] X. Xu and P. J. Antsaklis, "An approach for solving general switched linear quadratic optimal control problems," *Proc.* 40th IEEE International Conference on Decision and Control, pp. 2478–2483, 2001.

- [45] A. Giua, C. Seatzu, and C. van Der Me, "Optimal control of autonomous linear systems switched with a pre-assigned finite sequence," *Proc. IEEE International Symposium on Intelligent Control*, pp. 144–149, 2001.
- [46] X. Xu and P. J. Antsaklis, "Optimal control of switched autonomous systems," Proc. 41st IEEE International Conference on Decision and Control, pp. 4401–4406, 2002.
- [47] X. Xu and P. J. Antsaklis, "Optimal control of switched systems via nonlinear optimization based on direct differentiations of value functions," *International Journal of Control*, vol. 75, no. 16, pp. 1406–1426, 2002.
- [48] A. Bemporad, A. Giua, and C. Seatzu, "Synthesis of state feedback optimal controllers for continuous-time switched linear systems," *Proc.* 41st IEEE International Conference on Decision and Control, pp. 3182–3187, 2002.
- [49] A. Giua, C. Seatzu, and C. van Der Mee, "Optimal control of switched autonomous linear systems," *Proc.* 40th IEEE International Conference on Decision and Control, pp. 2472–2477, 2001.
- [50] A. Rantzer and M. Johansson, "Piecewise linear quadratic optimal control," *IEEE Transactions on Automatic Control*, vol. 45, no. 4, pp. 629–637, 2000.
- [51] S. Devasia, T. Meressi, B. Paden, and E. Bayo, "Piezoelectric actuator design for vibration suppression: Placement and sizing," AIAA Journal of Guidance, Control and Dynamics, pp. 859–864, 1993.
- [52] Z. Sun and D. Zheng, "On reachability and stabilization of switched linear control systems," *IEEE Transactions on Automatic Control*, vol. 46, no. 2, pp. 291–295, 2001.
- [53] Z. Yang, "An algebraic approach towards the controllability of controlled switching linear hybrid systems," *Automatica*, vol. 38, no. 7, pp. 1221–1228, 2002.
- [54] C. T. Chen, Linear System Theory and Design. Holt, Rhinehart, and Winston, Inc., New York, NY, 1984.
- [55] D. L. Kleinman and Athans, "The design of suboptimal linear time-varying systems," *IEEE Transactions on Automatic Control*, vol. 13, no. 2, pp. 15–159, 1968.

- [56] D. P. Bertsekas, "Note on the design of linear systems with piecewise constant feedback gains," *IEEE Transactions on Automatic Control*, vol. 15, no. 2, pp. 262–263, 1970.
- [57] "Mide technology corporation, medford, ma, http://www.mide.com,"
- [58] "Pcb piezotronics, inc., depew, ny, http://www.pcb.com,"
- [59] H. Khalil, "Nonlinear control systems," Prentice Hall, NJ., 2002.
- [60] D. O. Brush and B. O. Almroth, Buckling of Bars, Plates, and Shells. McGraw Hill, New York, 1975.
- [61] J. N. Reddy, An Introduction to the Finite Element Method. McGraw Hill, New York, 1993.
- [62] M. A. Langthjem and Y. Sugiyama, "Optimum design of cantilevered columns under the combined action of conservative and nonconservative loads part i: The undamped case," *Computers and Structures*, vol. 74, pp. 385–398.
- [63] H. P. Lee, "Divergence and flutter of a cantilever rod with an intermediate spring support," *International Journal of Solids and Structures*, vol. 32, no. 10, pp. 1371–1382, 1995.
- [64] "Micromo electronics, inc., clearwater, fl, http://www.micromo.com,"

